J Mater Sci: Mater Electron (2013) 24:3149–3169
DOI 10.1007/s10854-013-1240-0

REVIEW

Review on microstructure evolution in Sn–Ag–Cu solders and its effect on mechanical integrity of solder joints

Mrunali Sona · K. N. Prabhu

Received: 12 February 2013 / Accepted: 16 April 2013 / Published online: 5 May 2013

Abstract The use of Pb-bearing solders in electronic assemblies is avoided in many countries due to the inherent toxicity and environmental risks associated with lead. Although a number of "Pb-free" alloys have been invented, none of them meet all the standards generally satisfied by a conventional Pb–Sn alloy. A large number of reliability problems still exist with lead free solder joints. Solder joint reliability depends on mechanical strength, fatigue resistance, hardness, coefficient of thermal expansion which are influenced by the microstructure, type and morphology of inter metallic compounds (IMC). In recent years, Sn rich solders have been considered as suitable replacement for Pb bearing solders. The objective of this review is to study the evolution of microstructural phases in commonly used lead free xSn–yAg–zCu solders and the various factors such as substrate, minor alloying, mechanical and thermo-mechanical strains which affect the microstructure. A complete understanding of the mechanisms that determine the formation and growth of interfacial IMCs is essential for developing solder joints with high reliability. The data available in the open literature have been reviewed and discussed.

1 Introduction

Solder connects components in electronic devices and printed circuit boards through metallurgical bonding by providing necessary mechanical strength and conduction properties and finds extensive applications in electronic industries. Soldering is generally carried out at temperatures below 400 °C and solder has a melting point lower than the metals to be joined [1, 2]. The performance and quality of the solder are very important to the integrity of a solder joint, which in turn is vital to the overall functioning of the assembly. Sn–Pb solders have been widely used in almost all the electronic packaging industries as they are economical and have low melting point, good wettability and mechanical properties. Pb in solders gives outstanding properties to the overall reliability of the Sn–Pb solder, such as reduction of the surface tension of pure tin significantly and improves the wettability of solder alloy, Pb allows the rapid formation of inter metallic compounds (IMC) of Sn and Cu by diffusion, improvement in ductility, and prevention of transformation of β-tin (white tin) to α-tin (gray tin). If the transformation occurs, it will cause dramatic volume increase (about 26 %) and loss of structural integrity and hence loss of reliability. Low melting temperature of eutectic Sn–Pb (183 °C) solder, allows the use of a low reflow temperature in the electronic packaging process and ensures the reliability of the packages. As Pb is abundantly available in nature, it is economical to use in soldering alloys [3–5].

However, environmental concerns over the use of toxic Pb have lead to its ban in electronics manufacturing in most countries. A drop-in substitute for Pb should possess various desirable properties in terms of melting temperature, electrical and thermal conductivity, wettability, thermal expansion coefficient, mechanical strength, ductility, thermal fatigue resistance, creep resistance, manufacturability, workability, joint reliability and cost [6, 7]. Consideration must also be given to the health risks as well, while selecting alternative metals for Pb. Studies carried out in

M. Sona · K. N. Prabhu (✉)
Department of Metallurgical and Materials Engineering,
National Institute of Technology Karnataka, P.O. Srinivasnagar,
Surathkal 575 025, Karnataka State, India
e-mail: prabhukn_2002@yahoo.co.in

USA and Europe have shown that Cd is highly toxic. Sb should not be considered as a major alloying element as it is potentially carcinogenic. Ag, Cu, Bi, Sn and Zn are considered to pose low risk [8]. Among the numerous lead free solder alloys available, few families are of particular interest and prevailing choices of industry. Generally lead free solder alloys with melting temperature approximately below 230 °C are opted since they do not require any changes in process, boards or components that are used with conventional Sn–Pb solder. Eutectic or near eutectic compositions are preferred most, for having the least and single melting temperature [9].

Solder joint reliability is a measure of the ability of solder joint to perform its intended function under a set of service conditions for a given period of time. Therefore it can be reasonably assessed by the combination of service environment and system design. The service environment includes the temperature extremes which the product must withstand, possible mechanical and vibrational shocks the product may undergo and the frequency of power on/off cycling. Further from system design side, physical properties of the component and substrate, geometry of solder joint, the nature of IMCs formed and their structure, and mechanical properties of bulk solder alloy exert a significant effect on solder joint reliability [10, 11]. The formation of a strong and reliable solder joint is based on the ability of the liquid solder to uniformly and rapidly wet the surface finish and interact with it to form a consistent intermetallic layer at the interface [10]. The IMC layer provides a metallurgical bonding between the solder and the substrate. However, the IMCs are generally brittle, and it is frequently observed that fracture occurs at the IMC layers between the solder joint and the bonding pads. The thickness and morphology of IMC layers are considered to have a strong effect on the mechanical behaviour of the joints [12]. The ever increasing needs of high temperature performance, low cost, light weight and miniaturisation in electronic products demand improved solder joint reliability [12, 13]. With the desire for device miniaturization and increase in higher input/output (I/O) connections in packing, IC devices with high density substrates generate more heat during service. The heat is dissipated through the solder joints and this could result in a temperature increase in the joints. The temperature increase could accelerate the diffusion of elements across the solder joint interface, resulting in interfacial IMC layer growth. Therefore investigation of the microstructure and properties of the IMCs is essential to evaluate the mechanical behaviour and reliability of the solder joints [14]. Effects of various parameters such as Ag content, surface coating and alloying on mechanical behaviour and solder joint reliability are reviewed in the present paper.

2 The Sn–Ag–Cu lead free solder alloys

Among the various lead free solders available, SAC series alloys have emerged as highly accepted alloys. A survey by European lead free technology roadmap says that the near eutectic SAC alloys with a composition of 3–4 % Ag and 0.5–1 % Cu are the most popular and widely accepted solder alloys [15, 16]. Supply status of potential candidate elements for lead free solder applications are given in Table 1. Sn–Ag–Cu ternary alloy has the advantage of excellent wetting ability, good interfacial properties, high creep resistance, low coarsening rate and also relatively low melting temperatures compared to 96.5Sn–3.5Ag binary eutectic alloy. Addition of Cu lowers the melting temperature and improves the wettability of SAC solder alloys [5, 16]. Ternary phase diagram of Sn–Ag–Cu is shown in Fig. 1. The initial microstructure of lead free joints is highly influenced by the solidification process from the liquid state. The area indicated in the red box shows the near eutectic region. Most of the commercially available SAC alloy compositions are within this region [5]. The eutectic reaction takes place at a temperature of 217.2 °C. Under equilibrium solidification conditions, the microstructure of near-eutectic SAC solders consist three-phase ternary eutectic micro constituent, most likely consisting of a high volume fraction of β-Sn matrix containing small, needle, or disc-shaped particles of Ag_3Sn and Cu_6Sn_5 [19–22]. However, substantial deviation from uniform eutectic microstructure has been observed by many researchers. The equilibrium ternary eutectic phase transformation is suppressed in Sn–Ag–Cu alloys, due to a typically large undercooling of about 10–50 °C associated with the nucleation of the β-Sn phase. Hence the Ag_3Sn and Cu_6Sn_5 intermetallic precipitates sometimes can grow to large sizes before the whole joint solidifies. These are said to be primary precipitates and the remaining fine intermetallic precipitates between the β-Sn dendrites are referred to as secondary precipitates [23]. In the absence of the eutectic transformation, liquid alloys traverse metastable portions of the primary Ag_3Sn or Cu_6Sn_5 phase fields, yielding primary-like intermetallic phases and reducing the

Table 1 Supply status of potential candidate elements for lead free solder applications [18]

Element	World production (10^3 kg)	World capacity (10^3 kg)	Spare capacity (10^3 kg)
Ag	12,200	13,600	1,360
Bi	3,630	7,260	3,630
Cu	7,256,000	9,251,000	1,995,000
Ga	27	72	45
In	109	218	109

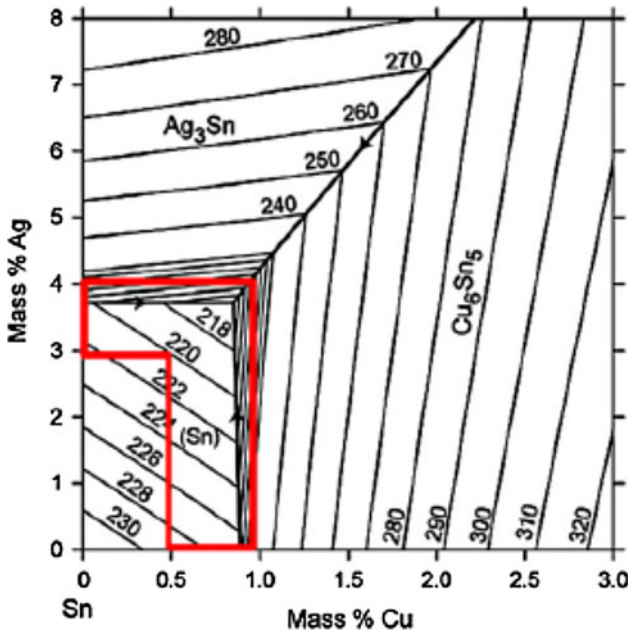

Fig. 1 Ternary phase diagram of Sn–Ag–Cu [16, 17]

Ag and Cu contents of the remaining liquid far below equilibrium values. Once β-Sn nucleation commences, the liquid alloy composition resides within the primary β-Sn region under conditions of large constitutional supercooling. This makes the β-Sn to adopt a dendritic morphology, and during dendrite growth interdendritic regions become enriched in Ag and Cu and eventually solidify as monovariant or invariant eutectic microconstituents, depending on local composition [21]. Microstructure of SAC bulk solder is shown in Fig. 2. To enhance the reliability of micro solder joints, understanding the interfacial microstructure is required. The formation of interfacial IMCs indicate good wetting and bonding properties, however massive IMCs present at the interface may decrease the mechanical properties of the entire joint [25, 26]. Mainly three IMCs namely Ag_3Sn, Cu_6Sn_5 and Cu_3Sn are formed at the solder joint as shown in Fig. 3. Reaction between Sn and Cu yields Cu_6Sn_5. Reaction between Sn and Ag results in the formation of Ag_3Sn but Cu_3Sn will not be found at the eutectic point until the Cu content is high enough for the formation of Cu_3Sn at higher temperatures, so Cu_3Sn is absent in bulk specimens. There exists no reaction between Ag and Cu to form any intermetallic [5, 16]. Ag_3Sn and Cu_6Sn_5 are said to possess much higher strength than the bulk solder material in SAC alloys whereas primary β-Sn phase has the lowest elastic modulus and yield strength among the bulk constituent phases in SAC alloys. Hence presence of large amount of Ag_3Sn and Cu_6Sn_5 phases result in a stiff bulk solder whereas high fraction of the primary β-Sn phase yields a soft and highly compliant bulk solder. Among the two types of IMC particles present in

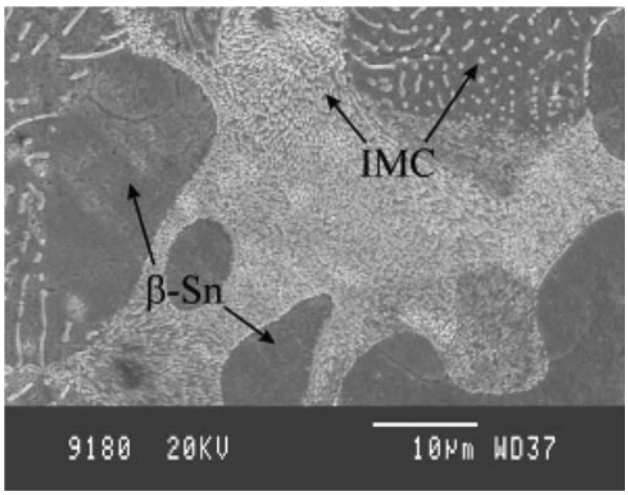

Fig. 2 Microstructure of SAC bulk solder [24]

the SAC solder alloys (Ag_3Sn and Cu_6Sn_5), it has been seen that the amount of Cu_6Sn_5 particles is much lesser than that of the Ag_3Sn particles. Ag_3Sn is the only Ag bearing phase present in the SAC solder. A increase in the amount of Ag content in SAC solders results in a quantitative increase of Ag_3Sn IMC particles formed [29–31].

3 Effect of various parameters on solder joint reliability

3.1 Effect of Ag content on IMC formation at the solder substrate interface

One of the highly focussed areas of research is the effect of Ag content of the Sn–Ag–Cu alloy on the interfacial microstructure and macro mechanical behaviour of the solder interconnects due to reliability concerns. The main concern is the existence of the large Ag_3Sn plates, which possess inherently in-compatible geometry to the surrounding microstructure, i.e. bulk solder and substrate. Cu is the most common conductor metal, which is utilized as substrate due to its good solderability characteristic and excellent thermal conductivity performance [32]. The Ag_3Sn appears at the interface between substrate and solder alloy when the Ag content is above 0.1 mass % [33].

Keller et al. [34] studied the mechanical properties of Sn–xAg–0.4cu/Cu joints by varying Ag content from 0 to 5 wt%. Shear tests were performed with four hypoeutectic (0–3 wt% Ag), an eutectic (3.7 wt% Ag) and two hypereutectic (4.5 and 5 wt% Ag) solder compositions. Figure 4 represents the shear strength of Sn–xAg–0.4Cu solder against Ag content. Specimen without containing any Ag content (Sn–0.4 wt% Cu) showed the lowest value (<20 MPa). Shear stress increased initially with the Ag

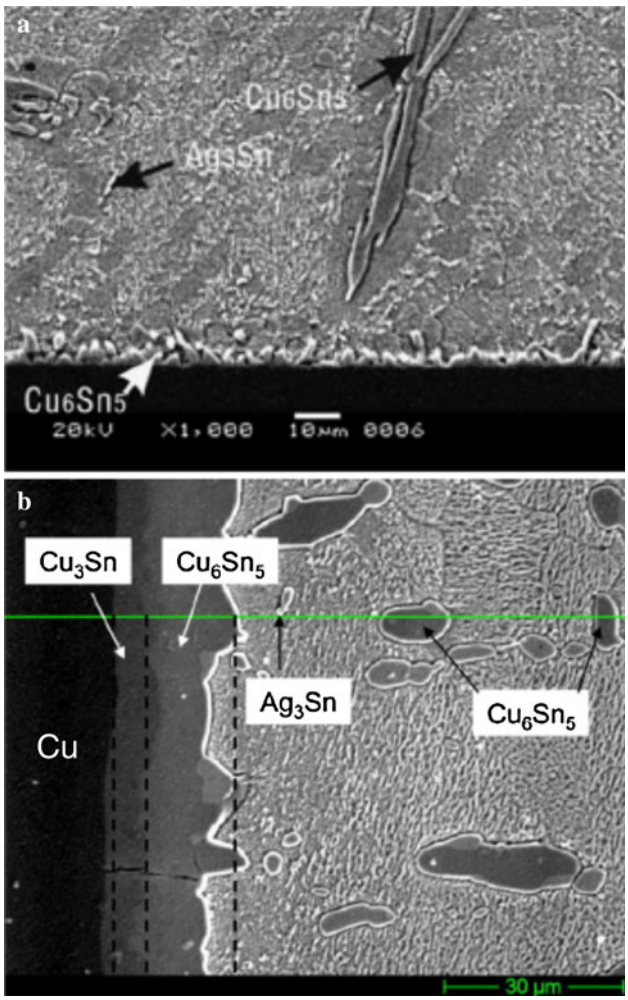

Fig. 3 **a** Microstructure of SAC/Cu solder joint after soldering for 30 s [27]. **b** Microstructure of SAC/Cu solder joint after aging [28]

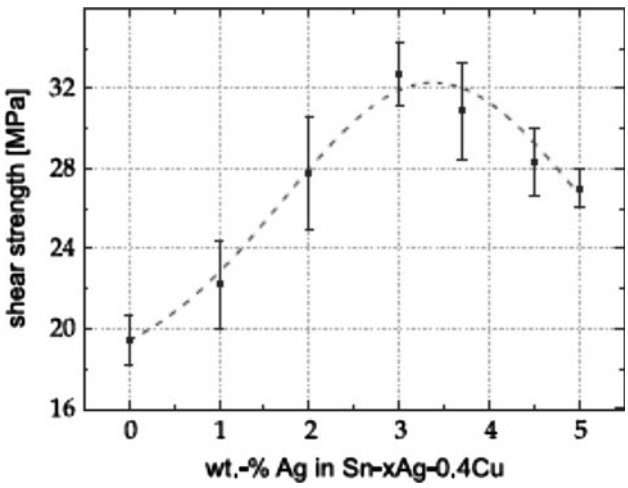

Fig. 4 Shear strength of Sn–xAg–0.4Cu solder against Ag content [34]

content and the curve reached a maximum at 3 wt% Ag and later declined slightly for eutectic and hypereutectic compositions. The maximum shear stress attained for Sn–3Ag–0.4Cu is about 32.5 MPa. Solder without any Ag content showed the maximum ductility. Vicker hardness values also showed a similar trend. There was increase in hardness values up to addition of 3 wt% Ag, later decreased with the increase of Ag content. The ideal soldering temperature leading to the maximum joint strength was found to be around 300 °C. After reflow at about 300 °C the microstructure of SnAgCu alloys consisted of sparse, huge primary precipitations, large areas of β-Sn dendrites and interdendritic regions, in which fine intermetallic particles were dispersed in a Sn matrix. The mechanical properties of the solder were mainly affected by the finer Ag_3Sn particles ($\approx$140 nm diameter) than the coarser Cu_6Sn_5 particles ($\approx$1 μm diameter) and were controlled by particle hardening within the interdendritic zones. Dislocation interaction with the small Ag_3Sn precipitates within the interdendritic zones plays the dominant role in solder strengthening. (1) particle shearing or (2) bypassing by bowing of dislocations (Orowan mechanism) are the two general mechanisms that control the strength, when particles hamper the movement of dislocations.

Kim et al. [35] studied the effect of alloy composition on microstructure by varying Ag and Cu composition of SAC alloy from 3.0 to 3.9 wt% and 0.5 to 0.7 wt% respectively. They found that the formation of large Ag_3Sn platelets degrade the mechanical properties of solder joints and also formation of Ag_3Sn platelets increase at the interface regardless of kind of the substrate used, with the increase of Ag content. Large Ag_3Sn platelets which appeared in Sn–3.5Ag–0.7Cu and Sn–3.9Ag–0.6Cu solders on Cu, Au/Ni/Cu, 42 alloy and stainless steel, induced brittle fracture at an interface and acted as crack initiation sites. They also noticed the formation long needle and hollow shaped Cu_6Sn_5 whiskers in all most all the solder–Cu joints and the high Cu content solder joints. For the high Cu content solder joints with a 42 alloy substrate, long Ni–Cu–Sn whiskers were formed at the interface and in the solder. The fracture surface of the Sn–3Ag–0.5Cu solder–Cu joints exhibited typical ductile fracture, whereas the other two alloys, Sn–3.5Ag–0.7Cu and Sn–3.9Ag–0.6Cu; showed a mixture of both ductile and brittle fractures. Large Ag_3Sn platelets did not form in alloys with less than 3.2 wt% Ag content. These large Ag_3Sn plates must be avoided as they provide crack initiation sites under tensile and shear stresses [36]. Since there is no way to detect where the Ag_3Sn plates form and in which direction they grow in solder joints, the practical way to subside their detrimental effect on solder joint reliability is to avoid their formation. This can be achieved by reducing the Ag content below its eutectic composition value 3.4 wt%. When the Ag content

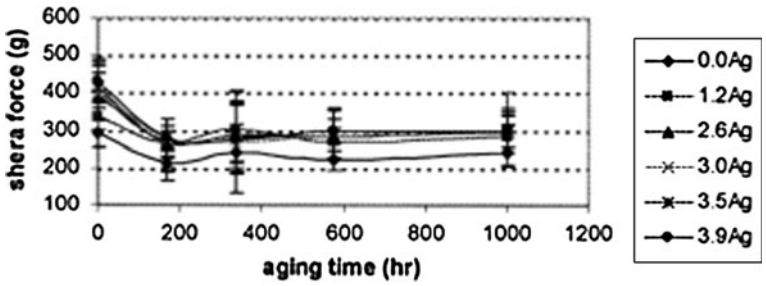

Fig. 5 The shear plot of the Sn–xAg–Cu interconnects through the isothermal aging [38]

is lower than the eutectic composition of 3.4 wt%, the Ag_3Sn phase forms as the secondary phase in the form of fibers. These Ag_3Sn fibers act as pins to hinder the motion of dislocations in the solder, making the solder more difficult to deform. High Ag content is desired for thermal cycling performance because of the strengthening effect of Ag_3Sn fibers, but it should not be higher than 3.4 wt%. Consequently, a Sn–Ag–Cu solder joint with lower Ag content can release more stress by plastic deformation of the bulk solder and thus perform better in drop, impact, high-speed bending, shearing, and pulling tests. Ag improves the resistance of the solder to thermal fatigue by forming Ag_3Sn fibers, but it has a negative effect on the interfacial reliability because the Ag_3Sn fibers make it more difficult for the joints to relax the stress. In a Sn–Ag–Cu solder joint on a Ni/Au-plated pad, if the content of Cu is higher than 0.3 wt%, the dual IMC structure of $(Cu,Ni)_6Sn_5/Ni_3Sn_4$ will form at the interface. It is suggested that this dual IMC structure at the interface contributes to the high interfacial failure rate of Pb-free packages. The solder joint would be able to tolerate high Ag content and would give high performance in both thermal cycling and drop tests if the Cu content is selected in such a way that dual IMC does not form at the interface [37].

Lu et al. [38] in their study on impact of Ag (0.0, 1.2, 2.6, 3.0, 3.5 and 3.9) on Sn–xAg–Cu solder, found a similar behaviour by the entire Ag alloy with regard to shear strength. They carried out isothermal aging (150 °C/1,000 h) of the test samples and found size reduction and sharp edge smoothening of the Ag_3Sn plates. The mechanisms of these phenomena are interpreted as via edge spheroidization and cylinderation of the Ag_3Sn plates during the aging. The corresponding mechanical shear performance of the inter connects did not degrade after the aging, regardless of the Ag content. For the first 24 h of aging there was a decrease in the shear strength and then a stable constant value was maintained throughout the rest of the aging process (Fig. 5). Zhang et al. [39] also noticed similar kind of shear force reduction in first 24 h of isothermal aging at 150 °C for Sn–3.5Ag–1.0Cu interconnects due to rapid coarsening of fine Ag_3Sn particles. Lu et al. [38] found a similar decrease in the shear strength during

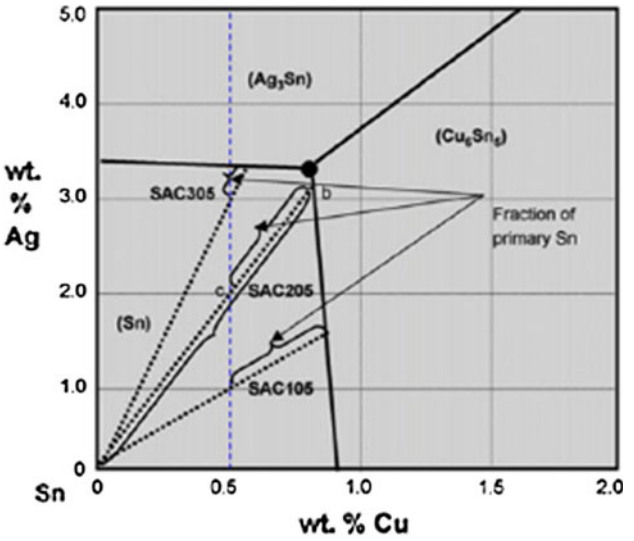

Fig. 6 Schematic diagram of Sn-rich region in the Sn–Ag–Cu ternary phase diagram [29]

first 24 h of aging for Sn–0.7Cu. They concluded that the change in bulk solder, mainly tin is the reason for initial decrease in the shear strength of lead free interconnects. The low Ag-content SAC alloys have been reported to yield more primary β-Sn phase, as shown in Fig. 6 [29, 40, 41]. Table 2 gives the shear strength of various Sn–Ag–Cu alloy compositions. It can be seen from these research works that an increase in Ag content from 3.2 wt% to any higher level does not offer any enhancement in mechanical properties. When Ag content is around 3–3.2 wt % the solder shows good temperature cycling reliability. The yield strength, tensile strength, shear strength and hardness show a maximum value. Plasticity suffers with increase of Ag content above 3 wt% but solidification cracks are the major problems in low Ag SAC solders. Solidification cracking occurs during the terminal stage of solidification, when the tensile stresses developed across adjacent grains exceed the strength of the almost completely solidified metal. Lu et al. [47] showed that solidification cracks exist in solder joints when the Ag content is between 1 and 3.0 wt%. They found no cracks in Sn–3.8Ag–0.7Cu solder joints. The total crack length of the Sn–Ag–Cu solder joints increased to a maximum and then droped to zero as Ag content increased from 1.0 to 3.8 wt %. Susceptibility to

solidification cracking ranged as follows: SAC207 > SAC305 > SAC107 > SAC387. This study is important for an appropriate solder selection for the electronic assemblies. For solder joints in important microelectronic assemblies, SAC387 is a better option due to its good solidification cracking resistance, despite its high cost.

3.2 Numerical modelling of growth behaviour of IMCs

A number of modelling techniques have been put forward by researchers to describe the growth behaviour of interfacial IMCs during soldering. IMC growth rate varies with different thermal cycling aging profiles such as isothermal aging, accelerated thermal cycling and thermal shock. Many researchers have found that IMC growth rate is higher during thermal shock and thermal cycling than isothermal aging [48]. IMCs grow during aging and strength of the solder joint decreases with the increase of IMCs size. The reason for this reduction in strength in solder alloys after aging must be due coarsening of microstructure. Based on experimental data, Hall and Petch found that the yield strength of a polycrystalline material is inversely proportional to its grain size as shown in the equation,

$$\sigma_y = \sigma_i + kd^{-0.5} \tag{1}$$

where σ_y is the yield strength of the polycrystalline material; σ_i is a constant for the material, it is the overall resistance of the lattice to dislocation movement; k is a constant which measures the contribution of hardening due to grain boundaries; and d is the grain size. The Hall–Petch theory states that increasing grain size reduces the strength of materials. The increasing grain size leads to decrease in the amount of grain boundaries. Therefore only fewer grain boundaries will be available to block the dislocation movement. Hence the material strength will be lost. The grain and phase structure coarsening is promoted by the self-diffusion of atoms, interstitials and vacancies.

According to the diffusion equation,

$$D = D_o \exp\left(-\frac{Q}{kT}\right) \tag{2}$$

where D is diffusivity, D_o is a constant that is independent of temperature, k is the Boltzmann constant, Q is the activation energy, and T is the absolute temperature, higher temperatures will increase the diffusivity of the atoms, interstitials and vacancies, leading to grain growth [5, 49].

Generally, the thickness of the IMC layer can be determined using a simple growth model,

$$x = (Dt)^n \tag{3}$$

where x is the IMC layer thickness at time t, D is the diffusion coefficient of the diffusing atomic species which determine the growth of the IMC layer and n is the time exponent. It can be assumed that the value of n is 0.5 when the reaction is mainly controlled by the diffusion mechanism. The thickness of the IMC layer (x) is plotted against $t^{0.5}$, to analyze the growth rate. D is determined from a linear regression analysis of x versus $t^{0.5}$, where the slope of the graph is $D^{0.5}$ [13, 27].

More precisely IMC layer thickness is measured using a relation [25]

$$x = x_o + kt^n \tag{4}$$

where x represents the thickness at time t, x_o is the IMC thickness for the as-soldered condition, t is the aging time, n is the power law exponent. The common form of this equation used to model the IMC growth is used with $n = 0.5$, corresponding to $D = k^{0.5}$. D is the usual diffusion coefficient; expressed in $m^2\ s^{-1}$.

$$x = x_o + \sqrt{Dt} \tag{5}$$

D varies with the temperature according to Arrhenius law. Layer growth is faster at higher aging temperature with the diffusion coefficient being given by Arrhenius equation represented by Eq. (2) [27, 49, 50]. Activation energy can be estimated and effect of temperature on growth rate can be evaluated by converting the Eq. (2) into the following form and by drawing Arrhenius plot of ln (D) versus $1/kT$.

$$\ln(D) = \ln(D_o) + \left(-\frac{Q}{kT}\right) \tag{6}$$

where k is the Boltzmann constant.

Therefore overall IMC layer growth kinetic is given by

$$x = x_o + A_o t^n \exp\left(-\frac{\Delta H}{RT}\right) \tag{7}$$

where A_o is the pre exponential diffusion factor, ΔH is the apparent activation energy for the growth, and R is the universal gas constant. The growth kinetic parameters of the IMC layer such as n, A, ΔH were determined by plotting the measured IMC layer thickness against the exposure time, at any given temperature. The data are fitted using a power law relationship given by Eq. 7 [51–54]. Equation 7 can be used only for isothermal conditions.

Experimental study of IMC layer growth between Sn3.8Ag0.7Cu and Ni/Au surface finish by isothermal aging versus thermal cycling (TC) aging was investigated by Xu et al. [55] to develop a framework for correlating IMC layer growth behaviour. An integrated model for IMC growth was derived to describe the Ni–Cu–Sn IMC growth behaviour subject to TC aging.

Temperature variation is a function of time for TC, and IMC thickness should be the accumulation of the interfacial reaction for different temperatures over accumulated

Table 2 Comparision of the shear strength of various SAC and Sn–Pb solder joints

Properties	Sn–Ag–Cu	Sn–Pb	References/Remarks
Shear strength (MPa)			At 0.1 mm/min
	27 (Sn–3.8Ag–0.7Cu)	23 (63Sn–37Pb)	20 °C
	17 (Sn–3.8Ag–0.7Cu)	14 (63Sn–37Pb)	100 °C
			Ref. [42]
			At 0.1 mm/min
	35.1 (Sn–3.8Ag–0.7Cu)	–	At room temperature
	18.2 (Sn–3.8Ag–0.7Cu)	–	125 °C
			Ref. [43]
	<20 (Sn–0Ag–0.4Cu)	≈20 (Sn–10 at. %Pb)	0.2 mm/s
	≈22 (Sn–1.0Ag–0.4Cu)	(Soldered at 250 °C)	Reflow temperature 340 °C
	≈28 (Sn–2.0Ag–0.4Cu)		Ref. [34]
	32.5 (Sn–3.0Ag–0.4Cu)		
	≈31 (Sn–3.7Ag–0.4Cu)		
	≈28.3 (Sn–4.5Ag–0.4Cu)		
	≈27 (Sn–5.0Ag–0.4Cu)		
	>24 (Sn–Ag–0.4Cu)	–	Reflow temperature 250 °C
	For Ag >2 wt.%		Ref. [34]
	9.8 (96.5Sn–3Ag–0.5Cu)	–	(On Au/Ni–P/Cu pad)
			Reflow temperature 220 °C
			Ref. [44]
			(On FR4 substrate)
	35 (95.5Sn–3.8Ag–0.7Cu)	–	At 25 °C
			Displacement rate 0.5 mm/min
	8 (95.5Sn–3.8Ag–0.7Cu)	–	At 125 °C
			Displacement rate 0.005 mm/min
			Ref. [45]
	≈55 (96.5Sn–3.0Ag–0.5Cu)	≈51 (63Sn–37Pb)	(On FR4 glass epoxy PCBs with OSP surface finish)
	≈61 (96.5Sn–3.8Ag–0.7Cu)	Reflowed at 222 °C for 37 s	Reflowed at 243 °C for 40 s
	≈52 (95.5Sn–4.0Ag–0.5Cu)		Tested at room temperature
			Displacement rate 2 mm/min
			Ref. [46]
	48 (96.5Sn–3.0Ag–0.5Cu)	≈44 (63Sn–37Pb)	(On FR4 glass epoxy PCBs with OSP surface finish)
	47 (96.5Sn–3.8Ag–0.7Cu)	Reflowed at 222 °C for 37 s	After aging at 85 °C for 1,000 h
	45 (95.5Sn–4.0Ag–0.5Cu)		Reflowed at 243 °C for 40 s
			Tested at room temperature
			Displacement rate 2 mm/min
			Ref. [46]
	≈46 (96.5Sn–3.0Ag–0.5Cu)	≈46 (63Sn–37Pb)	(On FR4 glass epoxy PCBs with NiAu surface finish)
	≈43 (96.5Sn–3.8Ag–0.7Cu)	Reflowed at 222 °C for 37 s	Reflowed at 243 °C for 40 s
	≈45 (95.5Sn–4.0Ag–0.5Cu)		Tested at room temperature
			Displacement rate 2 mm/min
			Ref. [46]
	≈43 (96.5Sn–3.0Ag–0.5Cu)	≈39 (63Sn–37Pb)	(On FR4 glass epoxy PCBs with NiAu surface finish)
	≈44 (96.5Sn–3.8Ag–0.7Cu)	Reflowed at 222 °C for 37 s	After aging at 85 °C for 1,000 h
	≈46 (95.5Sn–4.0Ag–0.5Cu)		Reflowed at 243 °C for 40 s
			Tested at room temperature
			Displacement rate 2 mm/min
			Ref. [46]
			At 0.1 mm/min test speed
	32 (Sn–0.5Ag–4Cu)	–	At room temperature
	40.5 (Sn–4.7Ag–1.7Cu)	–	At room temperature
	17.2 (Sn–4.7Ag–1.7Cu)	–	At 125 °C
			Ref. [43]
	67 (Sn–3.6Ag–1.0Cu)	36.5 (Sn–40Pb)	At 0.1 mm/min test speed
	58 (Sn–4.7Ag–1.7Cu)		Tested at 22 °C
	63.8 (Sn–3.8Ag–0.7Cu)		Ref. [42]

time. The layer growth rate, v, is a function of both temperature and time. ν is given by the following relationship.

$$v = \frac{dx}{dt} = \frac{1}{x^m} A' \exp\left(\frac{-\Delta H'}{RT}\right) \tag{8}$$

or,

$$x^m dx = A' \exp\left(\frac{-\Delta H'}{RT}\right) dt \tag{9}$$

Integration of Eq. 8, over the thickness x_o to x_t and time interval 0 to t gives,

$$\int_{x_o}^{x_t} x^m dx = \int_0^t A' \exp\left(-\frac{\Delta H'}{RT}\right) dt \tag{10}$$

Since Eq. 9 is applicable for any temperature profile T(t), to find the coefficient m, A' and $\Delta H'$, let T be a constant, and the integral formula is expressed as

$$x_t = x_o + [(m+1)A']^{\frac{1}{m+1}} \exp\left(-\frac{\Delta H'}{(1+m)RT}\right) t^{\frac{1}{m+1}} \tag{11}$$

Equation 11 and 7 are identical. Comparing these two equations, relationship between A_o and A', ΔH and $\Delta H'$, time exponents n and m can be found out. By substituting the values of A, ΔH and n in Eq. 10, the IMC growth corresponding to any temperature profile after any aging time can be predicted by,

$$x_t = x_o + \left[\frac{1}{n^2} A_o^n \int_0^t A' \exp\left(-\frac{\Delta H}{nRT}\right) dt\right]^n \tag{12}$$

Equation 12 can be used to calculate the IMC layer growth for any TC aging profile since n, A_o and ΔH can be easily found out through isothermal annealing. A simple approximation could be used to calculate the IMC thickness by numerical analysis,

$$x = x_o + A_o t_{eff}^n \exp\left(-\frac{\Delta H}{RT}\right) \tag{13}$$

where t_{eff} is the effective time and for most of the commonly used aging profiles, it is the total time at upper soak temperature [52].

Pang et al. [48] studied the morphology and growth of interfacial IMCs formed between 95.5Sn and 3.8Ag-0.7Cu and nickel/gold (Ni/Au) surface finish on BGA solder joint specimen. The growth behaviour of IMCs subjected to isothermal aging at 125 °C, thermal cycling (TC), and thermal shock (TS) with upper soak temperatures of 125 °C were compared. In order to simplify the comparison, the IMC growth was assumed to be volume diffusion controlled, i.e., the growth rate is proportional to the square root of time. They found that the effect of TS aging on IMC growth rate is more than TC aging. The TC aging has comparatively longer cycle time and soak period than TS aging and hence the stress relaxation at the solder joint is more pronounced in TC aging than TS aging. To quantify the acceleration effect of TC and TS aging, Pang et al. used another parameter, "equivalent isothermal aging time," t_{eq}, which is the time required by isothermal aging to obtain the same IMC thickness compared with TC or TS aging, and it is given by,

$$t_{eq} = \frac{1}{D_{iso}^2} (x_t - x_o)^2 \tag{14}$$

TC and TS are the most common tests used in checking the reliability electronic packaging. An acceleration factor, K is defined to relate the accelerated test (under TC and TS aging) compared to isothermal aging. It is the ratio of TC and TS, IMC growth to isothermal aging IMC growth. It is expressed as,

$$K = \frac{t_{eq}}{t_{eff}} \tag{15}$$

or,

$$K = \frac{1}{D_{iso}^2 t_{eff}} (x_t - x_o)^2 \tag{16}$$

The acceleration factor K is useful in reliability studies for correlating the IMC growth during TC, TS, and isothermal aging.

Dybkov [56] in his study on the growth kinetics of intermetallic layers at the interface of a solid metal and a liquid solder proposed mathematical equations to evaluate the thickness of any intermetallic layer formed under conditions of simultaneous dissolution in the under saturated solder melt. Growth of any intermetallic layer A_pB_q at the interface between a solid metal A and a liquid solder B saturated with A at a given temperature is a result of counter-diffusion of components A and B across its bulk and partial chemical reactions between diffusing atoms of one component and surface atoms of another component.

$$qB_{diffu\,sing} + pA_{surface} = A_pB_q \tag{17}$$

$$pA_{diffu\,sing} + qB_{surface} = A_pB_q \tag{18}$$

These reactions cause the increases, d_{xB1} and d_{xA2}, in layer thickness during a small period of time, dt, as shown in Fig. 7. The layer growth rate is given by,

$$\left(\frac{dx}{dt}\right)_{growth} = \frac{k_{0B1}}{1 + \frac{k_{0B1}X}{k_{1B1}}} + \frac{k_{0A2}}{1 + \frac{k_{0A2}X}{k_{1A2}}} \tag{19}$$

where k_{0B1} and k_{0A2} represents chemical constants; k_{1B1} and k_{1A2} represents diffusional constants (reaction–diffusion coefficients). The layergrowth kinetics are initially linear in the case of saturated solder melt (at x up to 500–600 nm) and then parabolic ($x > \sim 1$ μm) in the case of under saturated solder melt. The net rate of layer

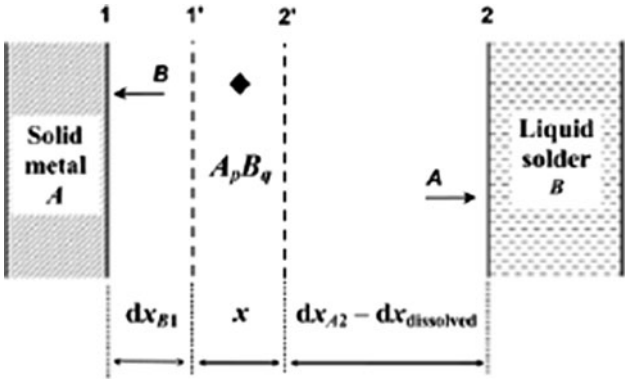

Fig. 7 Illustration of IMC layer growth process [56]

formation is the difference between the sum of the rates of its growth at interfaces 1 and 2 and the rate of dissolution at interface 2. The dissolution rate is given by,

$$\left(\frac{dx}{dt}\right)_{dissolution} = b_t = b_o \exp(-at) \tag{20}$$

where $b_o = C_s k/\rho\varphi$ and $a = ks/v$, C_s is the solubility of A in B at a given temperature. k represents dissolution rate constant, ρ is the density of the A_pB_q compound, ϕ is the content of A in A_pB_q in mass fractions, s is the surface area of the solid in contact with the liquid, and v is the volume of the liquid. Therefore a mathematical equation describing the A_pB_q growth kinetics at the A–B interface under conditions of dissolution in the liquid phase is given by,

$$\left(\frac{dx}{dt}\right)_{growth} = \frac{k_{0B1}}{1 + \frac{k_{0B1}X}{k_{1B1}}} + \frac{k_{0A2}}{1 + \frac{k_{0A2}X}{k_{1A2}}} - b_o \exp(-at) \tag{21}$$

Abdelhadi et al. [57] implemented Dybkovs model to investigate the growth kinetics of two compound layers during liquid–solid reactions such as the popular Cu–Sn reaction in soldering industry. The reacting liquid element is denoted by A and the solid element by B. Figure 8 shows the elements' regions and IMC regions in between these two elements. The growth regions at the interfaces are shown between 1 and 1′, 2 and 2′, 2 and 2″, and 3 and 3′. x and y represents IMC layer thickness for A_pB_q and A_rB_s IMC compounds accordingly. A_pB_q and A_rB_s are analogous to Cu_6Sn_5 and Cu_3Sn in Cu–Sn system. The following four chemical reactions within the interface regions are responsible for the growth of these two layers.

.

Layer formed	Interface	Partial chemical reaction	
A_pB_q	1–1′	$qB + pA = A_pB_q$	(22a)
	2′–2	$(sp - qr)A + qA_rB_s = sA_pB_q$	(22b)
A_rB_s	2–2″	$(sp - qr)B + rA_pB_q = pA_rB_s$	(22c)
	3′–3	$rA + sB = A_rB_s$	(22d)

Reaction (22a) governs the formation of the first IMC (A_pB_q) layer at the liquid interface and its growth from the original thickness x by the amount d_{xB1}. The numeric subscript represents the interface at which the reaction occurs and the alphabetic subscript indicates the diffusion element. At interface 2, each IMC layer transforms to the other IMC layer according to reactions (22b) and (22c). Reaction (22b) governs the formation of the first IMC layer by consuming the second IMC layer causing the thickness x of A_pB_q. IMC layer to increase by an amount dx_{A2}. Reaction (22c) represents the consumption of first IMC layer to form the second IMC layer A_rB_s causing a increase in layer thickness of y by an amount d_{yB2}. Reaction (22d) is responsible for the formation and growth of the second IMC layer at the interface 3. It causes the thickness y of second IMC layer to increase by d_{yA2}. Diffusion of atoms and subsequent chemical reactions are the two steps involved in each partial reactions discussed here. Therefore, the time (dt) required for increasing the thickness of any IMC layer by an amount dx, is the sum of the time of diffusion of the atoms of one of the components, through its bulk or other IMC layer, to the reaction site (dt_{dif}) and the time of their subsequent chemical reaction with the surface atoms (dt_{chem}) Therefore, following equations corresponding to equation (22) can be written:

$$dt = dt_{dif}^{B\to A_pB_q} + dt_{chem}^{B\to A_pB_q} \tag{23a}$$

$$dt = dt_{dif}^{A\to A_pB_q} + dt_{chem}^{A\to A_pB_q} \tag{23b}$$

$$dt = dt_{dif}^{B\to A_rB_S} + dt_{chem}^{B\to A_rB_S} \tag{23c}$$

$$dt = dt_{dif}^{A\to A_rB_S} + dt_{chem}^{A\to A_rB_S} \tag{23d}$$

By implementing Dybkovs assumptions that the time of diffusion of atoms (dt_{dif}) is directly proportional to both the change in the thickness of a layer and its existing total thickness and, the time of chemical reaction (dt_{chem}) is directly proportional to the change in the layer thickness and independent of its current thickness following equations are written.

$$dt = \left(\frac{x}{k_{1B1}} + \frac{1}{k_{0B1}}\right) dx_{B1} \tag{24a}$$

$$dt = \left(\frac{x}{k'_{1A2}} + \frac{1}{k'_{0A2}}\right) dx_{A2} \tag{24b}$$

$$dt = \left(\frac{x}{k'_{1B2}} + \frac{1}{k'_{0B2}}\right) dy_{B2} \tag{24c}$$

$$dt = \left(\frac{y}{k_{1A3}} + \frac{1}{k_{0A3}}\right) dy_{A3} \tag{24d}$$

All k_1 in these expressions represent diffusional rate constants, k_o represents chemical constants. The second subscript, A or B indicates the diffusing element and the

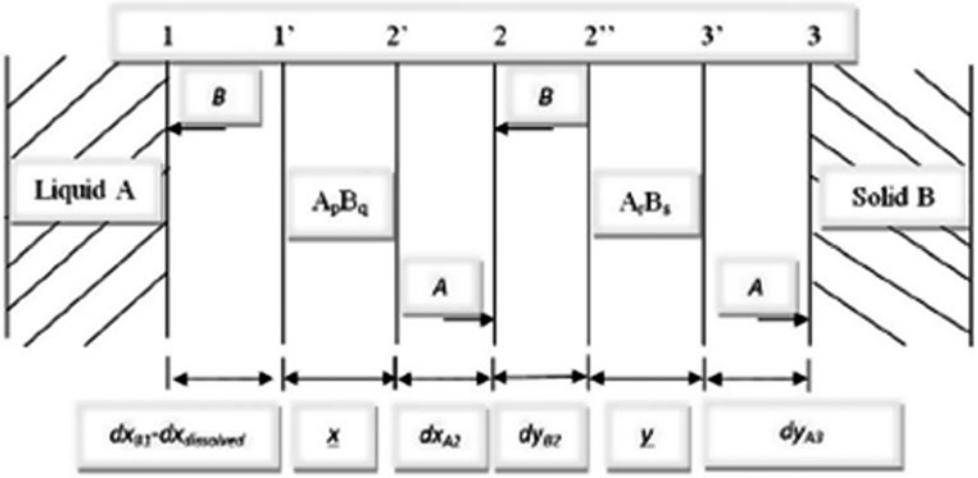

Fig. 8 Illustration of growth of A_pB_q and A_rB_s compounds between liquid A and solid B substances [57]

third numeric subscript indicates the interface at which the reaction occurs. k' is the converted form of the rate constant for chemical reactions represented by equations 22b and 22c taking into account the amount of atoms required by the chemical reaction.

$$k'_{1A2} = \frac{sp}{sp - qr} K_{1A2} \tag{25}$$

During the time dt the thickness of A_pB_q and A_rB_s increases by dx_+ and dy_+ respectively. However due to the reactions (22b and 22c) the thickness of layers A_pB_q and A_rB_s decreases by dx_- and dy_- respectively.

$$dx_+ = dx_{B1} + dx_{A2} \tag{26}$$

$$dy_+ = dy_{B2} + dy_{A3} \tag{27}$$

$$dx_- = \frac{rg}{p} dy_{B2} \tag{28}$$

$$dy_- = \frac{q}{sg} dx_{A2} \tag{29}$$

where g is the ratio of A_pB_q and A_rB_s molar volumes.

The layergrowth kinetics are described by a system of two equations of the form

$$\frac{dx}{dt} = \frac{k_{0B1}}{1 + \frac{k_{0B1}x}{k_{1B1}}} + \frac{k'_{0A2}}{1 + \frac{k'_{0A2}x}{k'_{1A2}}} - \frac{rg}{p} \frac{k'_{0B2}}{1 + \frac{k'_{0B2}y}{k'_{1B2}}} \tag{30}$$

$$\frac{dy}{dt} = \frac{k'_{0B2}}{1 + \frac{k'_{0B2}y}{k'_{1B2}}} + \frac{k_{0A3}}{1 + \frac{k_{0A3}y}{k_{1A3}}} - \frac{q}{sg} \frac{k'_{0A2}}{1 + \frac{k'_{0A2}x}{k'_{1A2}}} \tag{31}$$

The first two terms of each of these equations describe the rates of growth of an appropriate compound layer at its two interfaces, while the third term indicates the rate of consumption of this layer in the process of formation of an adjacent compound layer. In the case of the under saturated solder melt, the dissolution of the layer formed between liquid A and solid B occurs simultaneously with its growth. The overall change in thickness of the layer is therefore the difference between the rate of growth of the layer and the rate of its dissolution. Therefore the system of mathematical differential equations that describes the growth kinetics of two compounds under conditions of simultaneous dissolution in liquid phase A, are as follows:

$$\frac{dx}{dt} = \frac{k_{0B1}}{1 + \frac{k_{0B1}x}{k_{1B1}}} + \frac{k'_{0A2}}{1 + \frac{k'_{0A2}x}{k'_{1A2}}} - \frac{rg}{p} \frac{k'_{0B2}}{1 + \frac{k'_{0B2}y}{k'_{1B2}}} - \frac{C_S k_d}{\rho A_p B_q \varphi} \exp(-at) \tag{32}$$

$$\frac{dy}{dt} = \frac{k'_{0B2}}{1 + \frac{k'_{0B2}y}{k'_{1B2}}} + \frac{k_{0A3}}{1 + \frac{k_{0A3}y}{k_{1A3}}} - \frac{q}{sg} \frac{k'_{0A2}}{1 + \frac{k'_{0A2}x}{k'_{1A2}}} \tag{33}$$

where $a = k_d s/v$, k_d is the dissolution rate constant, s is the surface area of solid in contact with liquid, v is the volume of the liquid, C_s is the solubility of solid in liquid element at a given temperature and φ is the mass fraction of element B in A_pB_q compound. However developing a similar IMC growth model is complex for ternary alloy systems.

4 Substate surface finish

The manufactures use various surface finishes for example plating while soldering electronic devices on PCBs [35]. Whisker growth is a potential problem for the electronic product reliability. It is a surface relief phenomenon and whiskers relief the compressive stress in the matrix on which they grow. It has mainly arose on electroplated Tin. Tin whisker growth from vapor deposited tin surfaces has also been reported [9, 58–60]. Tin whisker is a conductive metal wire and it can grow over time with the use of tin plated or pure tin component finishes causing electrical shorts in the lead free solder. Tin whiskers can carry as high as 100 mA of current. Under some electrical/atmospheric conditions, whisker shorts may vaporize into conductive plasma of metal ions. Plasma forms arc capable of

carrying hundreds of amps resulting in catastrophic damage [61, 62]. There is no specific solution to prevent these whiskers. A thin layer of Ni can be electroplated before the electroplating of Sn, that is by creating a diffusion barrier between Sn and Cu whisker growth rate can be reduced. This method can be adopted because the room temperature reaction between Sn and Ni is much slower than between Sn and Cu. Another method is to use Cu-Sn compounds as diffusion barrier. Cu_6Sn_5 and Cu_3Sn compounds are good diffusion barriers to Cu diffusion at room temperature [9, 59].

Some researchers also observed that metal dopants such as Ni, could improve the solder joint drop performance by improving microstructure and property of Sn–Ag–Cu lead free solder [63]. These finishes influence the interfacial reaction and wetting properties. The thickness and composition of IMCs and reliability of solder joints are strongly influenced by surface finish layers. Cu is the most common conductor metal, which is utilized in contact with solders owing to its good solderability characteristic and excellent thermal conductivity performance. There exists two layers of Cu–Sn IMCs, Cu_6Sn_5 (thicker, adjacent to the bulk solder) and Cu_3Sn (thinner, adjacent to copper pad) between SAC and Cu pad under reflow durations. Cu_6Sn_5 IMC exhibits scallop-like morphology. The Cu–Sn interdiffusion process continues during solid state reaction. With the increase in aging time Cu_6Sn_5 becomes thicker and more uniform layer. Meanwhile, the thickness of Cu_3Sn layer also grows at the expense of Cu_6Sn_5. In addition, some voids were found at the Cu–Cu_3Sn interface and in the Cu_3Sn IMC layer after thermal aging for about 500–1,000 h above 100 °C [64]. For the two elements Cu and Sn, Cu is the dominant diffusing species through Cu_3Sn and Cu_6Sn_5. In the Cu–SAC solder reaction couple, the diffusing Cu atoms arrive at Cu_3Sn–Cu_6Sn_5 and Cu_6Sn_5-solder interfaces and result in the growth of both IMC layers towards the solder. Because of the unbalanced Cu–Sn inter diffusion through interface, atomic-level vacancies left by the migrating Cu atoms on the bare Cu side are not filled by Sn atoms. Theses vacancies coalesce into the so-called Kirkendall voids [32, 52, 65]. Voids reduce the mechanical properties of the board level interconnections and affect the conductivity performance and reliability of solder joints. Chiu et al. [66] found that for a bare Cu pad-SnAgCu solder interconnect system, Kirkendall voiding at the Cu and Cu_3Sn IMC interface is main mechanism for degradation of joint strength under thermal aging. The voiding process is activated at temperature as low as 100 °C. Since the interfacial voiding was shown to be detrimental to shock reliability of the system, Cu–SnAgCu solder system is not recommended to use in high temperature application. The growth rate of these voids are exponential with temperature and therefore increases significantly at higher temperatures particularly 125 °C and above, and these Kirkendall voids cause precipitous fall in solder joint reliability [49, 66].

Various surface finishes are applied to overcome these problems. Typical pad metallizations include elecroless nickel immersion gold (ENIG), organic solderability preservative (OSP), Ni–Au, Ni–Pd, immersion Sn (ImSn), immersion Ag (ImAg) etc. Song et al. [67] attached Sn–4.0 %Ag–0.5 %Cu on the package substrates with OSP and ENIG surface finish and found that IMC growth rates in solders on OSP surface finish is higher than that on ENIG. Ni–Cu–Sn ternary compound was found in SAC solder and found that Cu content in SAC solder decreased over the time of thermal aging at 150 °C. As a result $(Ni_{1-x}Cu_x)_3Sn_4$ was the main phase of IMC in the specimen after 500–1,000 h of thermal aging. The thickness of Ni–Cu–Sn IMC layer in samples with SAC solder on ENIG pads grew to 2 μm and 3.5 μm after 200 and 1,000 h of thermal aging at 150 °C respectively. With same testing condition Cu–Sn phase IMC layer in samples with SAC solder on OSP pads grew to 5.3 μm and 9 μm after 200–1,000 h of thermal aging indicating Ni layer in ENIG serves as a good barrier to inhibit detrimental growth of Cu-Sn IMC. Xu et al. [51] have studied the growth of interfacial IMCs and the interfacial voids/crack formation between 95.5Sn–3.8Ag–0.7Cu lead free solders and ENIG surface finish. The as reflowed IMC was a Sn–Ni–Cu ternary compound. Two different ternary Sn–Ni–Cu IMCs were, $(Cu_{1-x}Ni_x)_6Sn_5$ or $(Ni_{1-x}Cu_x)_3Sn_4$ [35, 48]. The Sn–Ni–Cu ternary IMC growth kinetics subjected to isothermal aging was determined at different temperature 150, 125 and 100 °C. The apparent activation energy ΔH was determined as 73 kJ/mol and a time exponent of 0.51 as shown in the following equation.

$$x = (1.35 \pm 0.2) \times 10^{-6} + 4.92t^{0.51\pm0.02} \exp\left[-(72.9 \pm 2.1) \times \frac{10^3}{RT}\right] \quad (34)$$

Compared with Sn/Cu system, the apparent activation energy ΔH for Sn/Ni is higher, hence its growth rate is slower. Hence, Ni is used as a barrier layer to prevent fast consumption of Cu substrate [51]. However, there are situations where rapid diffusion still exists through the breached regions in the nickel layer. To overcome this issue Ni layer is often coated with another layer of Au; also Au layer serves to protect against oxidation [14]. Doping Zn into Cu substrates has many advantages for soldering, such as the suppression of large Ag_3Sn compounds, the elimination of Cu_3Sn and Kirkendall voids during thermal aging, and the good drop, creep, and tensile resistances. Therefore it is expected that Zn containing Cu under bump metallization (UBM) can solve problems encountered in

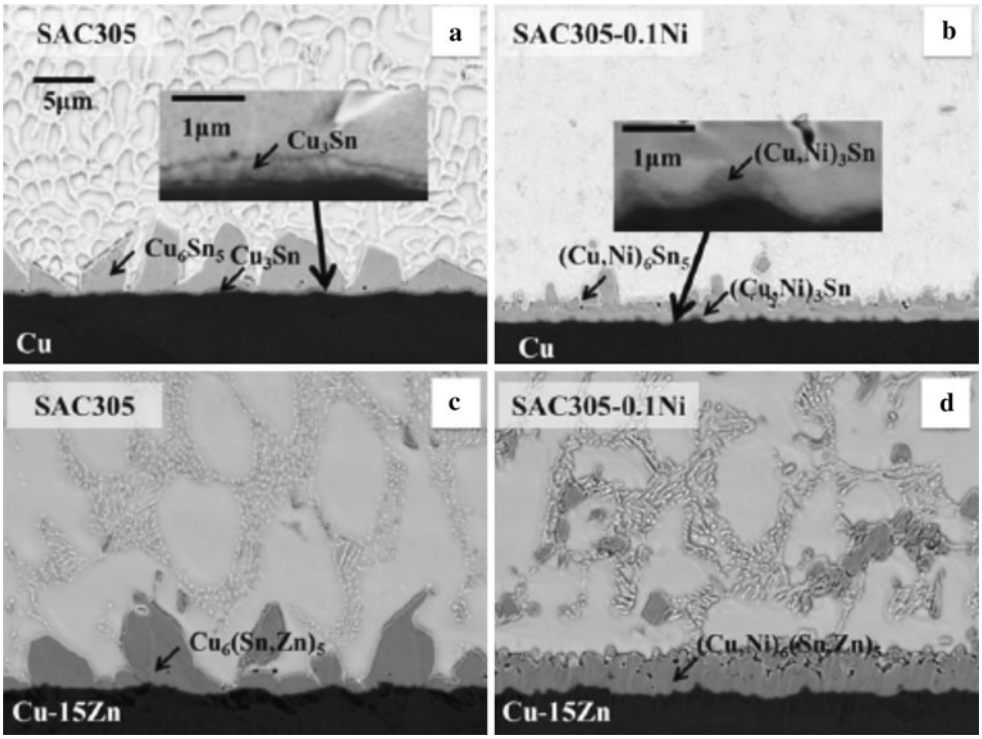

Fig. 9 SEM images of as reflowed **a** SAC305/Cu, **b** SAC305–0.1Ni/Cu, **c** SAC305/Cu–15Zn, and **d** SAC305–0.1Ni/Cu–15Zn interface [68]

Ni-doped solder joints. Chen et al. [68] studied the evolution of interfacial phase in Sn–3.0Ag–0.5Cu/Cu (wt%), Sn–3.0Ag–0.5Cu–0.1Ni/Cu, Sn–3.0Ag–0.5Cu/Cu–15Zn, and Sn–3.0Ag–0.5Cu–0.1Ni/Cu–15Zn solder joints. After reflow, scallop-type Cu_6Sn_5 and $Cu_6(Sn,Zn)_5$ was found at the SAC305/Cu and SAC305/Cu–15Zn interfaces respectively. Ni doped in the SAC305–0.1Ni/Cu and SAC305–0.1Ni/Cu–15Zn solder joints changed the morphology of IMCs from scallop-type to layer-type. Moreover, Zn diffused from the Cu–15Zn substrate to suppress the formation ofCu_3Sn at the SAC305/Cu–15Zn and SAC305–0.1Ni/Cu–15Zn interfaces while thin Cu_3Sn layer was present in the solder joints with Cu substrates. Figure 9 shows the as reflowed images of the interfaces of all four samples. During aging at 150 °C, a thick Cu_3Sn layer was observed at the interface between Cu_6Sn_5 and Cu substrate in the SAC305/Cu solder joint and many Kirkendall voids were present in the Cu_3Sn layer while in the SAC305–0.1Ni/Cu solder joint, a thin $(Cu,Ni)_3Sn$ formed at the interface and several Kirkendall voids were found in the $(Cu,Ni)_3Sn$ layer. SAC305/Cu–15Zn and SAC305–0.1Ni/Cu–15Zn solder joints, neither showed formation of any Cu_3Sn IMC layer nor Kirkendall voids even after aging at 150 °C for 960 h. The SAC305–0.1Ni/Cu–15Zn solder joint exhibited the thinnest and only one $(Cu,Ni)_6(Sn,Zn)_5$ IMC without any voids. The growth of interfacial $(Cu,Ni)_6(Sn,Zn)_5$ was insensitive to the solid state aging, owing to Zn and Ni re-distribution at the joint interface.

Kim et al. [69] used electroless nickel/electroless palladium/immersion gold (ENEPIG) surface finish and the mechanical strength of the SAC305/ENEPIG solder joints were investigated at various Pd thicknesses (0–0.5 μm). The $(Cu,Ni)_6Sn_5$ phase formed at the SAC/ENEPIG interface after reflow in all samples. $(Pd,Ni)Sn_4$ phase was found on$(Cu,Ni)_6Sn_5$ when the Pd thickness was almost equal or greater than 0.1 μm. A very thick layer of $(Pd,Ni)Sn_4$ was formed when Pd thickness was 0.3 μm. The interfacial strengths of the SAC/ENEPIG solder joints decreased under high strain rate due to weak interfacial fracture between $(Pd,Ni)Sn_4$ and $(Cu,Ni)_6Sn_5$ interfaces when the Pd thickness was greater than 0.3 μm. The mechanical strength of the SAC/ENEPIG solder joints was enhanced as the Pd thickness increased to 0.1 μm. Berthou et al. [25] studied aging of lead free assembled chip resistors and BGA, with either ENIG or immersion Sn finishes at 80 °C, 125 °C and 150 °C for 1,000 h and found that IMC thickness for a Sn PCB finish was higher than NiAu finish. This was again due to the nickel barrier. Hayes et al. [70] investigated the IMC growth associated with Sn–4.0Ag–0.5Cu solders on Ni–Au, Ni–Pd metallizations. $(Ni,Cu)_3Sn_4$ was present at the Ni interface for both the cases but was coarser and with greater variation in thickness in the case of Ni–Pd. Cu_6Sn_5 and Cu_3Sn were observed for both solder types. Wang et al. [71] used Sn3.0Ag0.5Cu solder doped with 0, 100, and 500 ppm Pd in his work and reflowed them on electroless Ni/immersion

Au substrate. During reflow process, Ni diffused into the solder alloy from substrate leading to the formation of needle-like $(Cu,Ni)_6Sn_5$ at the interface of the substrate and solder alloy. In comparison with SAC305–0Pd system, the thickness of $(Cu,Ni)_6Sn_5$ was found to be smaller in SAC305–0.05Pd. The Pd additive would trap Cu atoms and precipitated with Cu atoms as $(Cu,Pd)_6Sn_5$. Thus, the growth of interfacial $(Cu,Ni)_6Sn_5$ was restrained. In the Pd-doped system, $Cu_4Ni_2Sn_5$ grew continually at the SAC305–0.05Pd interface. In contrast, $Cu_4Ni_2Sn_5$ grew slowly and Cu_5NiSn_5 formed rapidly in the SnAC305–0Pd joint. This study provides a new SAC305 solder ball design with minor Pd doping, which could reduce the growth of $(Cu,Ni)_6Sn_5$ and promote the formation of stable $Cu_4Ni_2Sn_5$. Gu et al. [72] employed an electroless Ni–P–carbon nanotubes (Ni–P–CNTs) composite coating as a pad finish for electronic packaging. Electroless Ni–P and electroless Ni–P–CNTs composite coatings with the same P-contents were prepared. A Ni_3Sn_4 IMC layer and a P-rich layer were formed in the solder joints on both coatings after multiple reflows. The IMC layers were compact with chunky-shaped grains in SAC/Ni–P solder joints, whilst porous with needle-shaped grains in the case of SAC/Ni–P–CNTs solder joints. The CNTs dispersed in the Ni–P coating acted as a retardant in the reaction of the Ni with the solder hence growth rates of both the Ni_3Sn_4 IMC layer and the P richer layer in the SAC/Ni–P–CNTs solder joints were slower than those in the SAC/Ni–P solder joints. It was also found that the CNTs in the coating increased the brittleness of solder joints and weakened their shear strength. More brittle fractures occurred in the IMC layer in the Sn–4Ag–0.5Cu/Ni–P–CNTs solder joints during shearing tests. You et al. [73] studied the reliability of eutectic Sn–Pb, Sn–1.0Ag–0.5Cu, Sn–3.0Ag–0.5Cu and Sn–4.0Ag–0.5Cu solder bumps on 3 different pad surface finishes (ENIG, electrolytic Ni/Au and Cu–OSP) without and with an aging treatment at 150 °C for 100 h. The high-speed pull fracture test was conducted for the different samples with different surface finishes. From this study combination of SAC 105 solder ball and Ni-Au surface finish appeared to be the best option for enhanced impact reliability of BGA microelectronic package. Yoon et al. [74] created artificial voids by performing temperature humidity (TH) test of the substrate and studied the effect of isothermal aging and TH treatment of the substrate on joint reliability of Sn–3.0Ag–0.5Cu/OSP finished copper chip scale package solder joint and concluded that voids are formed by the oxidation or entrapped air of the OSP finished Cu substrate during TH test, because voids were not found on the substrates not subjected to TH test.

Choubey et al. [50] used Sn–3.0Ag–0.5Cu solder and ImAg, ImSn, OSP and ENIG pad finishes in their study and found that, after 350 h of aging at 125 °C, the IMC growth in the solder joints of the ImSn, ImAg and OSP were comparable, whereas the ENIG pad finishes showed a lower IMC thickness. After 1,000 h of aging at 100 °C, the IMC thickness was found to be approximately 3 μm, which was 1 μm less than the IMC thickness at 125 °C for the joints aged 1,000 h. In fact, the IMC growth for SAC305 at 350 h and 125 °C was significantly greater than the growth after 1,000 h at 100 °C. IMC thickness on various surface finishes is given in Table 3. ENIG is preferable for long-term reliability applications to ImSn, ImAg, and OSP finishes. OSP finish can be used for short-term reliability applications since it is economical compared with ImSn, ENIG, and ImAg, also results in comparable IMC thickness but applications prone to tin whisker formation should avoid ImSn finish. Care must be taken while using PCBs with an OSP finish since it is an organic finish and prone to contamination, which can lead to reliability problems. ImAg finish is highly sensitive to plating chemistry and hence is prone to champaign voids, and should be avoided as a primary choice for PCB finish [50].

5 Alloying elements

Addition of rare earth elements such as La, Ce, Lu and Y etc. to Sn rich solders was found to improve both the mechanical and physical properties. Rare earth elements can reduce the melting point of the solder, improve the wettability, depress the IMC growth and upgrade the shear strength and creep resistance of SnAgCu solder alloys [75]. Dudek et al. [76] have compared the mechanical properties of conventional SnAgCu with SnAgCu doped with La and Ce. It was found that small La and Ce additions (0.1 wt% and 0.5 wt%) to Sn–Ag–Cu results in a significant increase in ductility compared with Sn–Ag–Cu/Cu joints. At these small RE concentrations, homogenously distributed $RESn_3$ intermetallic phases form in the solders and they allow microscopic voids to nucleate, throughout the solder volume (instead of localized strain at the solder–intermetallic interface), and homogenize the strain in the solder joint thereby increase the ductility of the solder. During loading, force is transferred from the matrix to these slightly stiffer $RESn_3$ particles which act as second phase. Because they are compliant, it is likely that an appreciable amount of deformation takes place in these phases as well, contributing to the improvement in ductility. Figure 10 shows the as-processed optical images of (a) Sn–3.9Ag–0.7Cu–2La, (b) Sn–3.9Ag–0.7Cu–2Ce and (c) Sn–3.9Ag–0.7Cu–2Y respectively. Zhang et al. [77] found in their work that addition of 0.03 % Ce into SnAgCu alloy would contribute to the decrease of the thickness of IMC layer and the enhancement of the solder joint strength by analyzing the inter metallic layer of SnAgCu/Cu and SnAgCuCe/Cu [78].

Table 3 IMC thickness on various surface finishes

IMC thickness on Ni/Au PCB finish			
t = 0 h	t = 500 h (125 °C)	t = 1,000 h (125 °C)	Ref. [25]
≈1.75 μm	≈2.4 μm	≈2.5 μm	
t = 0 h	t = 500 h (150 °C)	t = 1,000 h (150 °C)	
≈1.75 μm	≈3 μm	≈3.6 μm	
IMC thickness on Sn PCB finish			
t = 0 h	t = 500 h (125 °C)	t = 1,000 h (125 °C)	Ref. [25]
≈3.9 μm	≈4.4 μm	≈5.1 μm	
t = 0 h	t = 500 h (150 °C)	t = 1,000 h (150 °C)	
≈3.9 μm	≈6.4 μm	≈8 μm	
Sn4.0Ag0.5Cu + OSP			
t = 0 h	t = 500 h (150 °C)	t = 1,000 h (150 °C)	Ref. [67]
≈2 μm	≈7 μm	≈9.1 μm	
Sn4.0Ag0.5Cu +ENIG			
t = 0 h	t = 500 h (150 °C)	t = 1,000 h (150 °C)	Ref. [67]
≈1.1 μm	≈2.6 μm	≈3.3 μm	
95.5Sn–3.8Ag–0.7Cu + ENIG			
t = 0 h	t = 250 h (150 °C)	t = 400 h (150 °C)	Ref. [25]
≈1.6 μm	≈6.9 μm	≈7.4 μm	
t = 0 h	t = 250 h (125 °C)	t = 400 h (125 °C)	
≈1.6 μm	≈2.8 μm	≈3 μm	
Sn–3.0Ag–0.5Cu + ENIG			
t = 0 h	t = 350 h (100 °C)	t = 1,000 h (100 °C)	Ref. [50]
≈1.5 μm	≈3.1 μm	≈3.3 μm	
t = 0 h	t = 350 h (125 °C)	t = 1,000 h (125 °C)	
–	≈2.8 μm	≈3.6 μm	
Sn–3.0Ag–0.5Cu + OSP			
t = 0 h	t = 350 h (125 °C)	t = 1,000 h (125 °C)	Ref. [50]
≈2.5 μm	≈3.4 μm	≈3.6 μm	
Sn–3.0Ag–0.5Cu + ImSn			
t = 0 h	t = 350 h (100 °C)	t = 1,000 h (100 °C)	Ref. [50]
≈2 μm	≈2.9 μm	≈3.1 μm	
t = 0 h	t = 350 h (125 °C)	t = 1,000 h (125 °C)	
≈2 μm	≈3.5 μm	≈4.3 μm	
Sn–3.0Ag–0.5Cu + ImAg			
t = 0 h	t = 350 h (100 °C)	t = 1,000 h (100 °C)	Ref. [50]
≈2.2 μm	≈2.7 μm	≈2.9 μm	
t = 0 h	t = 350 h (125 °C)	t = 1,000 h (125 °C)	
≈2.2 μm	≈3.85 μm	≈3.85 μm	

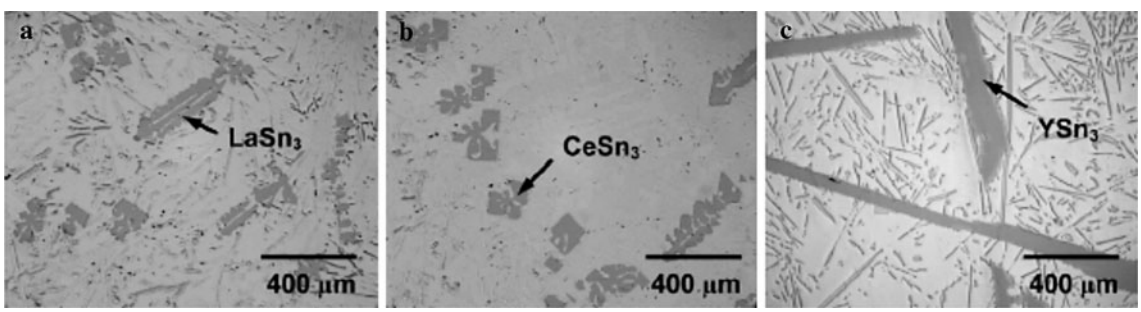

Fig. 10 As-processed optical images of **a** Sn–3.9Ag–0.7Cu–2La, **b** Sn–3.9Ag–0.7Cu–2Ce and **c** Sn–3.9Ag–0.7Cu–2Y [76]

It was found that the morphology of IMCs formed both at SnAgCu/Cu and SnAgCuCe/Cu interfaces gradually changed from scallop-like to planar-like, and different IMC thickness developed with increasing aging time. The activation energy for the IMC growth during aging was found to be 73.5 kJ/mol for SnAgCu/Cu and 89.4 for SnAgCuCe/Cu showing the IMC growth rate was higher for the SnAgCu/Cu system than for the SnAgCuCe/Cu system [77]. Xie et al. [79] studied the reliability performance of Ce-containing Sn–3.9Ag–0.7Cu/Cu and Ni–P joints under isothermal aging at 95 °C for 250 h. Interfacial intermetallic layer $(Cu,Ni)_6Sn_5$ was formed between both Sn–3.9Ag–0.7Cu and Sn–3.9Ag–0.7Cu–0.5Ce solder on Ni–P. Monotonic shear results of as reflowed joints showed that Ce-containing Sn–3.9Ag–0.7Cu joints exhibit enhanced ductility on both Cu and Ni–P substrates. Ce-containing Sn–3.9Ag–0.7Cu has excellent oxidation resistance, and also the mechanical performance of Ce-containing joints does not degrade on isothermal aging. It is known that the standard Gibbs free energy of formation for Sn–RE IMCs is lower than those for Cu–RE and Ag–RE. So the RE elements have a higher affinity for Sn, and this explains their effectiveness in the refinement of the Sn–rich microstructure. Wu et al. [24] found in his work that the addition of 0.25 % RE elements of mainly cerium (Ce) and lanthanum (La), to Sn–3.5Ag–0.7Cu have refined the coarse β-Sn grains and the IMC particles. Anderson et al. [80] studied the strength of SAC solder matrix by the addition of a fourth alloy (x = Mn, Ni, Ge, Ti, Si, Cr and Zn). SAC + X alloys were based on Sn–3.7Ag–0.9Cu (wt%), where the X element was assumed to enter the alloy as a substitution for Cu. In the as-soldered and 100 h aged at 150 °C conditions, the solder joint shear strength values were grouped closely, with the exception of the as-soldered joint samples made from Sn–3.7Ag–0.53Cu–0.37Ge with an average shear strength of about 57 MPa, which was more than 20 % above the next highest average shear strength. It was notable that after 1,000 h of aging at 150 °C, shear strength values of all the modified SAC + X alloy joints were stronger than the Sn–3.7Ag–0.9Cu solder alloy, which served as the base composition. If all alloy results are averaged, the maximum shear strength of these Pb-free solder joints dropped by about 19.3 % from the as-soldered condition to the 100 h aged condition when SAC + Ge was not included. The average shear strength dropped only by another 13 % from the 100 h aged condition to the 1,000 h aged condition. Thus, after 1,000 h of aging at 150 °C, the average maximum shear strength of the solder joints made from all the alloys in this study retained more than two thirds of the as-soldered maximum shear strength. In addition, Lai et al. [81] found that the addition of Ni alters the interfacial IMC structure while Ge enhances the mechanical behaviour of the bulk solder. Although SnAgCu lead free solder provides better mechanical properties, thermal fatigue behaviour than the conventional SnPbsolder it faces surface oxidation and shrinkage cracking problem. This problem could be overcome by adding Ni and Ge. Ge is very effective in preventing oxidation of Sn at surface of molten SAC lead free solder. Ni is effective in improving the mechanical properties. The creep behaviour of Sn–3.5Ag–0.5Cu–Ni–0.01Ge was found to be better than SAC solder. Ni suppresses the growth of Cu_3Sn IMC layer. Cu_3Sn is scarcely sensitive to Ni in the range of 0.07–0.25 mass % [82]. The addition of Ni favors the formation of fiber-like IMCs and finer dot-shaped precipitates on the surface of β-Sn matrix rather than needle-like morphology. The addition of 0.06 wt % Ni and 0.5 wt % Sb into SAC105 resulted in a significant improvement in creep resistance of about 210 and 350 % when compared with the SAC105 solder alloy [83]. Addition of Bi and Ni prominently improves the shear strength of SAC0705 solder joints. This enhancement partially depends on the solid solution strengthening and dispersion strengthening of Bi and Ni in the bulk solder, which significantly increases the integrated intensity of the solder joints [84].

Gain et al. [85] added a small amount of Ni and Al nano-particles to Sn–3.0Ag–0.5Cu solder alloy to investigate its effect on the formation, growth and evolution of the IMC layer structure at OSP-Cu pad/solder interfaces. A Sn–Ni–Cu IMC layer was formed at the interfaces in solder joints containing Ni nano-particles. Aging at 150 °C for various aging times resulted in a very thin Cu_3Sn IMC layer between Sn–Ni–Cu IMC layer and OSP–Cu pads. Cu_6Sn_5 and Cu_3Sn IMC layers were clearly observed in solder joints containing Al nano-particles. The aged Sn–Ag–Cu–0.5Ni solder joints had a suppressed formation of the Cu_3Sn IMC layer due to the continuous formation of the Sn–Ni–Cu IMC layer when compared Sn–Ag–Cu–0.5Al/OSP–Cu. The formation of Sn–Ni–Cu IMC particles was also responsible for a consistently higher hardness of solder joints containing Ni nano-particles. Dong et al. [75] studied the effect of addition of trace amounts of Ni (0.1 wt%), P (0.01 wt%) and Ce (0.05 wt%) to SAC 305 individually. They found a decrease in wettability of SAC305 solder alloy with the addition of Ni and Ce whereas increase in wettability with the addition of P. They could also observe a depression in hot crack formation on the solder surface with the addition of Ni and Ce elements whereas P element additions aggravated the hot cracking of solder. Oxidation resistance of solder was increased with the Ni addition but Ce element addition worsened the anti-oxidation property. However, P significantly improved the anti-oxidation property of SAC305 solder.

Kang et al. [86] found that the minor Zn addition to SAC alloy can reduce their amount of undercooling during

solidification and hence can suppress the formation of large Ag_3Sn plates. Wang et al. [87] observed granular Cu–Zn on the surface of Sn3.0Ag0.5Cu1.0Zn/Cu when compared with scallop shaped Cu_6Sn_5 in Sn3.0Ag0.5Cu/Cu and the Cu_5Zn_8 grain size of the SnAgCuZn solder was much smaller than the Cu_6Sn_5 grain size of the SnAgCu solder. Daly et al. [88] in their study on Ni and Zn-doped Sn–2.0Ag–0.5Cu lead free solders, found a delay in the formation of Ag_3Sn until all the Ni and Zn elements were consumed to form $(Cu,Ni)_6Sn_5$ and Cu_6Zn_5 IMC phases respectively. The addition of 0.05Ni and 0.5Zn to SAC(205) alloy resulted in an increase in YS and UTS as well as the ductility at all temperatures and strain rates. The formations of new $(Cu,Ni)_6Sn_5$ and Cu_6Zn_5 IMCs have been recognized to reinforce the solder matrix and decrease the β-Sn grain size. It was also found that that the strengthening effect of Ni was not as strong as that of Zn. Kotadia et al. [89] found the formation of $(Cu,Zn)_6Sn_5$ IMC at the interface for 0.5–1 wt% Zn. When the Zn concentration was 1.5 wt% a Cu_5Zn_8 IMC layer was observed followed by massive spalling leaving the more thermodynamically stable Cu_6Sn_5 IMC to form at the Cu/solder interface. SAC–Zn solder alloy formed $(Cu,Ni,Zn)_6Sn_5$ IMC instead of $(Cu,Ni)_6Sn_5$ on Ni–P substrate. The higher Zn concentration solder alloys also showed Ni_5Zn_{21} IMC grains close to the interface and Ni–Cu–Sn–Zn–Au particles embedded into interfacial IMC. The $(Cu,Ni,Zn)_6Sn_5$ IMC layer found to grow with aging time but the growth rate on Ni–P substrate was significantly lower than on Cu substrate. The lowest growth rate was found in the SAC–1.5Zn/Ni system. In the joints made from the modified Sn–3.9Ag–0.9Cu solders, the Co substitution appeared to catalyze nucleation and growth of primary Cu_6Sn_5, similar to the Sn–3.6Ag–1.0Cu solder joints. In contrast, the Fe substitution appeared to produce highly refined Sn dendrites, far finer than those in joints made from Sn–3.0Ag–0.5Cu, Sn–3.9Ag–0.6Cu, and the unmodified Sn–3.7Ag–0.9Cu [80]. Fallahi et al. [90] investigated the influence of adding In, Ce and Fe to Sn–3.6Ag–0.9Cu. A reliability tests on four compositions, SAC, SAC–0.2Fe, SAC–0.6Fe and SAC–1.7In–0.3Ce, showed that adding In and Ce was effective in improving the mechanical properties of the solder on the Ni–P substrate. Adding In and Ce, and Fe was found to improve the shear strength. The improvement in shear strength was due to the decrease in wetting angle with the addition of In and Ce, and Fe. It was also found that Fe refines the microstructure by increasing amount of undercooling or lowering activity of Sn leading to better solder joint. SAC–InCe showed better ductility with a good strength on the Cu substrate. For the solder on the Ni–P substrate, SAC–0.6Fe and SAC–0.2Fe had the highest maximum stress of about 42 MPa whereas for the solders on Cu substrate the final strengths were 53 MPa and 40 MPa for SAC–0.6Fe and SAC–0.2Fe respectively. However, for both substrates, the fracture strain of SAC–InCe was higher than that of SAC–0.6Fe despite of its higher strength. The addition of In and Ce, and Fe found to be more effective in increasing fracture toughness than shear strength. Shnawah et al. [91] found that the Fe (0.1–0.3 wt%) addition to the SAC105 bulk solder alloy, further increases the bulk compliance and the plastic energy dissipation ability of the solder joints, which plays an important role in drop impact performance enhancement. Chuang et al. [92] found that the addition of a small amount of Ti slightly decreases the melting temperature range of the SAC solder alloy and effectively refines the microstructure. The coarse β-Sn grains in Sn3.5Ag0.5Cu alloy become finer and uniform, the eutectic colony becomes narrower, and the new Ti_2Sn_3 IMC develops. The UTS, 0.2YS and microhardness of the SAC–XTi solder found to increase with increase in alloying Ti content from 0.25 to 1.0 wt%. Elongation was found to decrease when the Ti content exceeded 1.0 wt%.

Composite approaches are also given by researchers to improve the reliability of solder joints. Haseeb et al. [93] found that addition molybdenum nano-particles to SAC solder impart their influence on the interfacial IMC as discrete particles. They do not appear to dissolve or react with the solder. They tend to adsorb preferentially at the interface between solder and the IMC scallops and hinder the diffusion flux of the substrate and thereby suppress the IMC growth. Rao et al. [94] added nano sized Mo particles to Sn–3.8Ag–Cu (SAC387) to form a composite and studied the effect of the strain rate on tensile deformation characteristics and found that yield strength and strain hardening exponent increased with strain rate. Liu et al. [95] added 20 nm moissanite SiC particles to Sn–3.8Ag–0.7Cu solder paste and found a decrease in the size of β-Sn sub grains and the IMCs when compared with solders without SiC nano-particles. This was due to the strong adsorption effect and high surface free energy of the SiC nano-particles. They also found an improvement in the microhardness of SAC + 0.05 wt% SiC composite by about 44 % when compared with the non composite. Further increase in the addition of SiC to the matrix resulted in the entanglement of SiC particles in the bulk solder. Therefore, a significant reduction in the IMC size was not observed in the composites containing more than 0.05 wt% SiC nano-particles.

Carbon nanotubes (CNTs) are widely known to have exceptional and attractive physical, thermal, electrical and mechanical properties. CNTs possess almost 100 times the tensile strength ($\approx$150 GPa) of high-strength steel alloys. These extraordinary unique qualities make them suitable for making many novel composites to overcome the performance limits of conventional materials [96, 97]. Nai

et al. [14, 96, 98] used 95.8Sn–3.5Ag–0.7Cu with particle size of about 25–45 μm as matrix alloy and multiwall carbon nanotubes (MWCNT) of 3–20 nm outer diameter and length <100 μm as fillers. The composite solder joints showed lower diffusion coefficient when compared to monolithic solder joints indicating the presence of CNTs as reinforcements in solder joints was effective in retarding the growth of the IMC. In order to achieve efficient load-transfer during loading, it is essential to have good interfacial bonding between the CNTs and the solder matrix. However, for composite solder materials, the formation of CNT clusters in the solder matrix could hinder effective bonding between the CNTs and the solder particles. Therefore, at higher amount of CNT additions (0.04 and 0.07 wt%), Nai et al. observed only a marginal improvement in the strength value as compared to that of monolithic solder joint. This could also be associated with the higher level of microporosity observed at higher weight percentage of CNTs.

Han et al. [99–101] incorporated Ni coated multiwall carbon nanotubes to Sn–3.5Ag–0.7Cu composite solder and observed an improvement of about 8 % in 0.2 % yield strength and 12 % in ultimate tensile strength with the incorporation of 0.05 wt% Ni–CNTs to Sn–3.5Ag–0.7Cu. Reduction in mechanical properties were observed for the addition of Ni-CNTs beyond 0.05 wt% due to the formation of CNT clusters. They used Ni–CNT incorporated Sn–3.5Ag–0.7Cu composite solder with Au/Ni/Cu substrate in another work. Ni was chosen because of its good wetting characteristics with SAC alloys and as it can form stable phases (Ni_3Sn_4) in the Ni–Sn binary system. With the addition of Ni-coated CNTs, the interfacial IMC thickness of the composite solder joints were observed to grow slower than that of the monolithic SAC solder joints. Significant improvement was observed with the addition of 0.05 wt% of Ni–CNTs, for which the ultimate shear stress values increased by 29 % under the as-soldered condition and by 44 % after subjected to 2,000 thermal cycles (from −40 to +125 °C). Generation of geometrically necessary dislocations to accommodate thermal and elastic modulus mismatch between solder matrix and Ni–CNTs, load-transfer due to the presence of Ni–CNTs and thinner IMC layer in the composite solder joints were the reasons for the enhanced mechanical properties. The interfacial microstructure and shear strength of SAC and SAC/Ni–CNT solders on Ni/Au-finished pads were also investigated after aging at 150 °C for up to 42 days. Both as-soldered and isothermally aged composite solder joints showed ultimate shear strength superior to that of their monolithic counterparts. Significant improvement was observed with the addition of 0.05 wt% of Ni–CNTs, for which the ultimate shear stress values increased by 29 % (as-soldered) and 28 % (aged for 42 days), respectively. The shear strength of all the aged solder joints decreased with increasing aging duration. Bukat et al. [102] used functionalization and esterification methods for the structural modification of multiwall carbon nanotubes. Esterification was performed via the Fischer esterification method using methanol or polyethylene glycol. The modified carbon nanotubes appeared to be thinner and longer as compared to initial MWCNTs. A negative effect of different types of carbon nanotubes, as well as concentration, was observed on the wetting results on FR-4 with a Cu substrate at 250 °C in contradiction to the observations of Nai et al. [14]. Only for the smallest concentration of esterified carbon nanotubes, especially for Functionalized Carbon Nano Tubes by polyethylene glycol (FCNTPG), smooth and shiny areas that were covered with the solder alloy were observed. Bukat et al. conclude that wetting phenomenon is due to the binding of solder grains by the carbon nanotubes, CNTs do not directly involve in the metallurgical reaction between the solder and the copper substrate. This inhibits the metallurgical reaction between the solder and the copper during reflow and mechanically disperses the CNTs between the solder grains, during the cooling process after the reflow. A reduction in the IMC thickness after the reflow of solder paste was found and this process was less intense in the case of FCNTPG.

Kumar et al. [97, 103] added single wall carbon nanotubes (SWCNT) to Sn–3.8Ag–0.7Cu solder and observed a increase in UTS and hardness with the increase of SWCNT up to 1 wt%. The nanotubes were found to be distributed at the edges of grain boundaries of Ag_3Sn intermetallic.The enhanced mechanical properties can be attributed to the effective load-transfer between the solder matrix and the nanotubes. The effect of brittle reinforcement content on strength and ductility of the composite solder can be explained by the strengthening mechanisms such as stress gathering capability of the reinforcing particles, increase in dislocation density, thermally induced matrix work hardening, and significant reduction in the average size/morphology of the secondary phases of the composite solder with the increasing wt% addition of nanotubes. To date, studies by several researchers have shown that, addition of CNTs into conventional solder alloy, convincingly improves the performance. However, researchers are not yet able to take out the full advantage of outstanding properties of CNTs due to few limiting factors, for instance: (1) the difficulty of homogeneously dispersing CNTs in the metal-based matrix, and (2) insufficient bonding at the nanotube– matrix interface. Research has to be carried out to overcome these problems [101].

It is found that addition of dioxide nano powders such as TiO_2, $Zr0_2$etc improves the strength of solder joints. Tsao noted that addition of 0.5 wt% nano TiO_2 to Sn–3.5Ag–0.5Cu suppresses the growth of IMCs. The reduced

diffusion coefficient of SAC composite solder/Cu joints to SAC composite/Cu joints indicated the positive result of nano TiO_2 addition. A stronger affinity of Ag and Sn in the case of nano TiO_2 addition into SAC solder increases the precipitation or adsorption of Ag_3Sn nano-particles on Cu_6Sn_5 grain surface and may decrease the activity of Sn atoms effectively suppressing the growth of overall IMC layer. Due to dispersion strengthening, the ultimate tensile strength, yield strength and microhardness of the composite solder increases with increase in TiO_2 content from 0.25 to 1 wt%. However, the ductility decreases because of the microporosity at the Ag_3Sn grain boundary. The morphology of Cu_6Sn_5 IMCs formed at temperature ranging from 250 to 325 °C between Sn–3.5Ag–0.5Cu–0.5wt% nano TiO_2 solder/Cu substrate was scallop shaped (mainly formed below 300 °C) and those formed between 300 and 325 °C were prism shaped. After aging for 7 days at temperature 100, 125, 150, 175 °C scallop shape changed to layer type [104–106].

Chang et al. [107] investigated the effect of addition of Al_2O_3 nano-particles on the formation and growth of interfacial IMCs between the Sn3.0Ag0.7Cu–0.5 Al_2O_3 composite solder and Cu substrate. Figure 11 shows the microstructure of the SAC solder and SAC–0.5 Al_2O_3 composite solder in the as-cast condition. As illustrated in Fig. 11a, near-eutectic SAC solder showed an off-eutectic microstructure comprising β-Sn dendrites and interdendritic regions with eutectic phases, i.e. β-Sn, Ag_3Sn and Cu_6Sn_5 whereas addition of Al_2O_3 nano-particles, refined the Ag_3Sn IMC size as shown in Fig. 11b. The reason may be that Al_2O_3 nano-particles promote a high nucleation density of the second phase in the eutectic colony during solidification. Addition of 0.5 wt% Al_2O_3 resulted in the change of morphology of IMCs from a continuous elongated scallop-shape at SAC/Cu interfaces to a discontinuous rounded scallop-shape at SAC–0.5Al_2O_3/Cu interfaces. The activation energies calculated for the overall IMC layers were 44.2 kJ/mol for SAC/Cu and 59.3 kJ/mol for SAC–0.5Al_2O_3/Cu soldering, respectively. The increase in the value of activation energy indicates that the addition of Al_2O_3 suppresses the growth rate of the IMC layer. Cheng et al. [108] studied the effect of addition of 0.25 wt% Al_2O_3 nano-particles to Sn3.5AgO.5Cu (SAC) solder, on evolution of microstructure between the solder and ImSn pad BGA substrates as well as shear strength as a function of multiple reflow cycles. A continuous, flated-type Cu_6Sn_5 IMC layer was observed in both SAC solder and SAC composite solder after 1st reflow. After 8 reflow cycles, the morphology of the Cu_6Sn_5 IMC layer changed from flated-type to rough prism type in SAC solder/Cu joints whereas flated-type to scallop-type in SAC composite solder/Cu joints. The SAC composite solder joints consistently displayed higher shear strength than that of SAC solder joints due to a second phase dispersion strengthening mechanism. The average shear strength of the SAC composite solder joints after 8 cycles of reflow found to be lower than that of the SAC composite solder joints after the first reflow cycle by about 8.4 % in SAC solder and 5.1 % in SAC composite solder. The shear strengths of SAC solder joints were lower than those of SAC composite solder joints after eight reflow cycles due to the presence of coarse Cu_6Sn_5 IMC in the solder matrix which could cause severe embrittlement and act as stress concentrators.

Fouzder et al. [109] studied the influence of $SrTiO_3$ nano-particles on the microstructure and shear strength of SAC solder on Au/Ni metallized Cu pads and found that addition of 0.5 wt% $SrTiO_3$ to Sn–3.0Ag–0.5Cu improves the shear strength of the solder joint. This was due to the second phase dispersion strengthening mechanism and refinement of Cu_6Sn_5, Ag_3Sn and $AuSn_4$ (IMCs) as well. $SrTiO_3$nano-particles are found to be dispersed throughout the β-matrix. The fine IMCs and $SrTiO_3$nano-particles improve the mechanical properties of the solder joint by pinning the grain boundaries. The solder joints containing $SrTiO_3$nano-particles underwent a ductile fracture with a very rough surface due to uniform dispersion of $SnTiO_3$-nano-particles. Gain et al. [110] found that addition of ZrO_2 to SAC (Sn–3.0Ag–0.5Cu) solder improves the shear

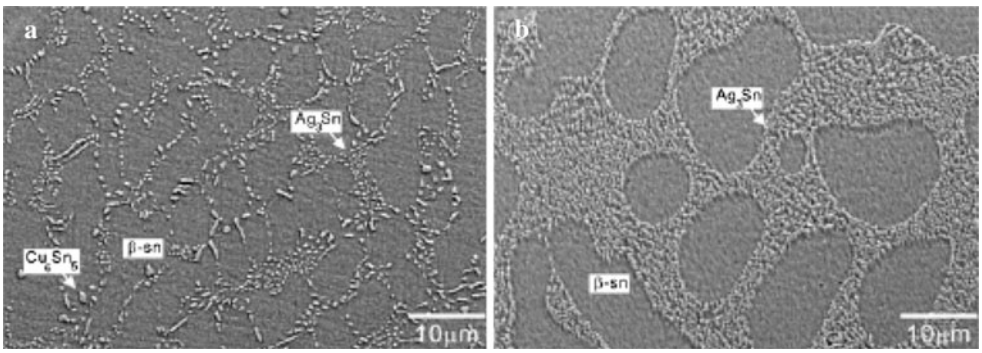

Fig. 11 SEM images of as-cast lead free SAC composite solders: (**a**) SAC, and (**b**) SAC-0.5Al_2O_3 [107]

strength of the solder joint. ZrO_2 has few advantages over other nano-particles. For example, density of ZrO_2 is 5.83 g/cm^3 which is almost similar to that for SAC, (density of Sn–3.0Ag–0.5Cu is 7.11 g/cm^3) when compared to other ceramic particles such as Al_2O_3 (3.97 g/cm^3) and SWCNT (1.3 g/cm^3). ZrO_2 has higher hardness than Sn–3.0Ag–0.5Cu. The microstructure of Sn–Ag–Cu solder on Au/Ni metallized Cu pad has Ag_3Sn, Cu_6Sn_5 and $AuSn_4$ IMC particles distributed in the β-Sn matrix whereas SAC composite solder containing ZrO_2nano-particles has uniformly distributed ZrO_2nano-particles in the β-Sn matrix in addition to the microstructure of unreinforced SAC solder alloy. The thickness of IMCs found to be increased from 2.8 μm to 6.7 μm for unreinforced SAC solder joints and for the solder joint with 3 wt% ZrO_2nano-particles it increased from 2 μm to 5.2 μm after the reflow process. The shear strengths of unreinforced SAC solder and solder joints with 3 wt% ZrO_2nano-particles after one reflow cycle were 38 and 43.4 MPa respectively. The corresponding values after 16 reflow cycles were 31.6 and 40.9 MPa respectively. At any number of reflow cycles the solder joints with high ZrO_2 nano-particles showed a consistently higher strength than that of the one with lower percentage of ZrO_2 nano-particles. Thus, it is confirmed that ZrO_2 nano-particles resist the formation of IMC layers and growth as well. ZrO_2 nano-particles may alter the driving force for the growth of the IMC layer and the diffusivity of elements involved in its growth. The ZrO_2 nano-particles may get adsorbed at the grain boundary and vary the relative relationship of the growth velocities between crystalline directions of IMC particles. This in turn, reduces the IMC particle size. Thus, addition of alloying elements and composite approach have great potential to improve the microstructure and hence mechanical properties of lead free solders.

6 Summary

Design and development of new lead free solders require a good understanding of the evolution of microstructure, IMC formation at the interface and their interaction. Evolution of microstructure in lead free solders has a significant influence on their mechanical and electrical properties. The formation of IMC is necessary for proper wetting of the solder to the substrate. However, massive IMCs present at the interface decrease the mechanical properties of the entire joint. SAC alloys are the most attractive lead free solders because of their better mechanical properties and thermal fatigue behaviour than the conventional Sn–Pb solder. Sn–xAg–Cu solders with high Ag content ($x > 3$ mass%) are reported to give good temperature cycling reliability but poor drop impact reliability whereas Sn–xAg–Cu solders with low Ag content ($x < 2$ mass%) show poor temperature cycling reliability but good drop impact reliability. Therefore, most semiconductor package assemblers are forced to implement multiple lead free alloys depending on intended performance. Limitations of SAC solders can be overcome either by alloying or by composite approach. Addition of rare earth elements bring down the rate of formation of the IMC layers by changing the diffusion coefficient. The addition of second phase nano-particles change the driving force for growth of intermetallic layer as well as the diffusivity of the elements involved in its growth. Nano-particles get adsorbed at the grain boundary and vary the relative relationship of growth velocities between crystalline directions of IMC particles leading to a reduction in the size of IMC particles. Nickel plays a dual role in soldering. It acts as good diffusion barrier and also slows down the growth rate of IMCs which are prone to crack formation. A knowledge of the effect of soldering process variables and aging on IMC morphology and evolution of microstructure is essential for accurate prediction of reliability of solder joints.

Acknowledgments Authors thank the Defence Research Development Organization (DRDO), Govt. of India, New Delhi for the financial support under a research grant: ERIP/ER/1006009M/01/356.

References

1. J. Kim, S. Jung, Int. J. Solids Struct. **43**, 1928 (2006)
2. T. Chellaih, G. Kumar, K.N. Prabhu, Mater. Des. **28**, 1006 (2007)
3. G. Kumar, K.N. Prabhu, J. ASTM Int. **7**, 1 (2010)
4. M. Abtewa, G. Selvaduray, Mater. Sci. Eng. **27**, 95 (2000)
5. H. Ma, J.C. Suhling, J. Mater. Sci. **44**, 1141 (2009)
6. M.E. Alama, S.M.L. Nai, M. Gupta, J. Alloys Compd. **476**, 199 (2009)
7. L. Zhang, J. Han, C. He, Y. Guo, J. Mater. Sci.: Mater. Electron. **24**, 172 (2013)
8. A.Z. Miric, A. Grusd, Solder Surf Mt Tech. **10**, 19 (1998)
9. K. Zeng, K.N. Tu, Mater. Sci. Eng., R **38**, 55 (2002)
10. Solder Joint Reliability, (ROHM and HAAS electronic materials circuit board technologies technical communications 2008), http://www.pcb007.com
11. J.S. Hwang, in *Implementing lead free electronics*, (McGraw-Hill, United States of America, 2005), p. 411
12. H. Tsukamoto, T. Nishimura, S. Suenaga, K. Nogita, Mater. Sci. Eng., B **171**, 162 (2010)
13. C.M.T. Law, C.M.L. Wu, D.Q. Yu, L. Wang, J.K.L. Lai, J. Electron. Mater. **35**, 89 (2006)
14. S.M.L. Nai, J. Weib, M. Gupta, J. Alloys Compd. **473**, 100 (2009)
15. Soldertec at Tin technology (European lead free technology roadmap, ver. 1, 2002), http://www.lead-free.org
16. D.A. Shnawah, M.F.M. Sabri, I.A. Badruddin, Microelectron. Reliab. **52**, 90 (2012)
17. K.W. Moon, W.J. Boettinger, U.R. Kattner, F.S. Biancaniello, C.A. Handwerker, J. Electron. Mater. **29**, 1122 (2000)
18. Q. Wang, W.F. Gail, R.W. Johnson, *Mechanical Properties and Microstructure Investigation of Lead Free Solder* (Auburn University, Auburn, 2005)

19. S.K. Kang, W.K. Choi, D.Y. Slii.I.L. Donald, W. Henderson, T. Gosselin, A.Sarkhel, C. Goldsmith, K.J. Punlitz, in *Proceedings of the Electronic Components and Technology Conference*, 2003, pp. 64–70
20. D. Lewis, S. Allen, M. Notis, A. Scotch, J. Electron. Mater. **31**, 61 (2002)
21. A.L. Londe, D. Emelander, J. Jeannette, C. Larson, W. Rietz, D. Swenson, D.W. Henderson, J. Electron. Mater. **33**, 1545 (2004)
22. U.R. Kattner, JOM 45 (2002)
23. L. Yin, L. Wentlent, L. Yang, B. Arfaei, A. Oasaimeh, P. Borgesen, J. Electron. Mater. **41**, 241 (2012)
24. C.M.L. Wu, D.Q. Yu, C.M.T. Law, L. Wang, Mater. Sci. Eng., R **44**, 1 (2004)
25. M. Berthou, P. Retailleau, H. Fremont, A.G. Gracia, C.J. Davennel, Microelectron. Reliab. **49**, 1267 (2009)
26. Z. Huang, Paul P. Conway, R.C. Thomson, Microelectron. Reliab. 47,1997 (2007)
27. D.Q. Yu, L. Wang, J. Alloys Compd. **458**, 542 (2008)
28. E. Hodulova, M. Palcut, E. Lechovic, B. Simekova, K. Ulricha, J. Alloys Compd. **509**, 7052 (2011)
29. D.A. Shnawah, S.B.M. Said, M.F.M. Sabri, I.A. Badruddin, F.X. Che, J. Electron. Mater. **41**, 2631 (2012)
30. M. Reid, J. Punch, M. Collins, C. Ryan, Solder Surf Mt Tech. **20**, 3 (2008)
31. Y. Kariya, T. Hosoi, S. Terashima, M. Tanaka, M. Otsuka, J. Electron. Mater. **33**, 321 (2004)
32. C.Y. Liu, K.N. Tu, T.T. Sheng, C.H. Tung, D.R. Frear, P. Elenius, J. Appl. Phys. **87**, 750 (2000)
33. C. Liu, C. Lai, M. Wang, M. Hon, J. Cryst. Growth **290**, 103 (2006)
34. J. Keller, D. Baither, U. Wilke, G. Schmitz, Acta Mater. **59**, 2731 (2011)
35. K.S. Kim, S.H. Huh, K. Suganuma, J. Alloys Compd. **352**, 226 (2003)
36. K.S. Kim, S.H. Huh, K. Suganuma, Mater. Sci. Eng., A **333**, 106 (2002)
37. K. Zeng, M. Pierce, H. Miyazaki, B. Holdford, J. Electron. Mater. **41**, 253 (2012)
38. H.Y. Lu, H. Balkan, K.Y. Simon, J. Mater. Sci.: Mater. Electron. **17**, 171 (2006)
39. F. Zhang, M. Li, B. Balakrisnan, W.T. Chen, J. Electron. Mater. **31**, 1256 (2002)
40. J.H. Lee, A.M. Yu, J.H. Kim, M.S. Kim, N. Kang, Met. Mater. Int. **14**, 649 (2008)
41. D. Suh, D.W. Kim, P. Liu, H. Kim, J.A. Weninger, C.M. Kumar, A. Prasad, B.W. Grimsley, H.B. Tejada, Mater. Sci. Eng., A **595**, 460 (2007)
42. Prevailing lead free solder, www.digitalengineeringlibrary.com
43. Database for properties of lead free solder alloys, Version 1.0, pp. 1–113
44. S. Chang, Y. Huang, Y. Lin, J. Alloys Compd. **490**, 508 (2010)
45. J.H.L. Pang, T.H. Low, B.S. Xiong, X. Luhua, C.C. Neo, Thin Solid Films **462**, 370 (2004)
46. J.J. Sundelin, S.T. Nurmi, T.K. Lepisto, E.O. Ristolainen, Mater. Sci. Eng., A **420**, 55 (2006)
47. W. Lu, Y. Shi, Y. Lei, J. Electron. Mater. **39**, 1298 (2010)
48. J.H.L. Pang, L. Xu, X.Q. Shi, W. Zhou, S.L. Ngoh, J. Electron. Mater. **33**, 1219 (2004)
49. G. Zeng, S. Xue, L. Zhang, L. Gao, W. Dai, J. Luo, J. Mater. Sci.: Mater. Electron. **21**, 421 (2010)
50. A. Choubey, H. Yu, M. Osterman, M. Pecht, F. Yun, L. Yonghong, X. Ming, J. Electron. Mater. **37**, 1130 (2008)
51. L. Xu, J.H.L. Pang, F.X. Che, in *Proceedings of the Electronic Components and Technology Conference*, 2005, pp. 682–686
52. L. Xu, J.H.L. Pang, in *Proceedings of the Electronic Components and Technology Conference*, 2006, pp. 275–282
53. J. Yoon, S. Jung, J. Mat. Sci. **39**, 4211 (2004)
54. P.T. Vianco, J.A. Rejent, P.F. Hlava, J. Electron. Mater. **33**, 991 (2004)
55. L. Xu, J.H.L. Pang, K.H. Prakash, T.H. Low, IEEE Trans. Compon. Packag. Technol. **28**, 1521 (2005)
56. V.I. Dybkov, JOM 76 (2009)
57. O.M. Abdelhadi, L. Ladani, J. Alloys Compd. **537**, 87 (2012)
58. B. Jiang, A. Xian, J. Mater. Sci.: Mater. Electron. **18**, 513 (2007)
59. J.W. Osenbach, J.M. DeLucca, B.D. Potteiger, A. Amin, F.A. Baiocchi, J. Mater. Sci.: Mater. Electron. **18**, 283 (2007)
60. M. Liu, A.P. Xian, J. Electron. Mater. **38**, 2353 (2009)
61. J. Pan, J. Wang, D. Shaddock, Int Microelectron Packag Soc. **2**, 72 (2005)
62. H. Leidecker, Tin whiskers, A history of documented electrical system failures, (http://nepp.nasa.gov/whisker/reference/tech_papers/2006-Leidecker-Tin-Whisker-Failures)
63. F.X. Che, E.C. Poh, W.H. Zhu, B.S. Xiong, in *Proceedings of the 9th Electronics Packaging Technology Conference*, 2007, pp. 713–718
64. D. Kim, J. Chang, J. Park, J.J. Pak, J. Mater. Sci.: Mater. Electron. **22**, 703 (2011)
65. Z. Mei, M. Ahmad, M. Hu, in *Proceedings of the Electronic Components and Technology Conference USA*, 2005
66. T. Chiu, K. Zeng, R. Stierman, D. Edwards, K. Ano, in *Proceedings of the Electronic Components and Technology Conference*, 2004, pp. 1256–1262
67. F. Song, S.W.R. Lee, in *Proceedings of the Electronic Components and Technology Conference*, 2006, pp. 1196–1203
68. W. Chen, C. Yu, J. Duh, J. Mater. Sci. **47**, 4012 (2012)
69. Y.M. Kim, J. Park, Y. Kim, J. Electron. Mater. **41**, 763 (2012)
70. S.M. Hayes, N. Chawla, D.R. Frear, Microelectron. Reliab. **49**, 269 (2009)
71. I.T. Wang, J.G. Duh, C.Y. Cheng, J. Wang, Mater. Sci. Eng., B **177**, 278 (2012)
72. X. Gu, Y.C. Chan, D. Yang, B.Y. Wu, J. Alloys Compd. **468**, 553 (2009)
73. T. You, Y. Kim, W. Jung, J. Moon, H. Choe, J. Alloys Compd. **486**, 242 (2009)
74. J. Yoon, B. Noh, Y. Lee, H. Lee, S. Jung, Microelectron. Reliab. **48**, 1864 (2008)
75. W. Dong, Y. Shi, Y. Lei, Z. Xia, F. Guo, J. Mater. Sci.: Mater. Electron. **20**, 1008 (2009)
76. M.A. Dudek, N. Chawla, Intermetallics **18**, 1016 (2010)
77. L. Zhang, S.B. Xue, G. Zeng, L.L. Gao, H. Ye, J. Alloys Compd. **510**, 38 (2012)
78. L. Gao, S. Xue, L. Zhang, Z. Sheng, F. Ji, W. Dai, S. Yu, G. Zeng, Microelectron. Eng. **87**, 2025 (2010)
79. H. Xie, N. Chawla, K. Mirpuri, J. Electron. Mater. **41**, 3249 (2012)
80. I.E. Anderson, J.L. Harringa, J. Electron. Mater. **35**, 91 (2006)
81. Y.S. Lai, J.M. Song, H.C. Chuang, Y.T. Chiu, J. Electron. Mater. **37**, 201 (2008)
82. H. Watanabe, N. Hidaka, I. Shoji, M. Ito, Mater. Sci. Technol. 135 (2006)
83. A.A.E. Daly, A.E. Hammad, A. Fawzy, D.A. Nasrallh, Mater. Des. **43**, 40 (2013)
84. Y. Liu, F. Sun, H. Zhang, J. Mater. Sci.: Mater. Electron. **23**, 1705 (2012)
85. A.K. Gain, Y.C. Chan, Intermetallics **29**, 48 (2012)
86. S.K. Kang, D.Y. Shih, D. Leonard, D.W. Henderson, T. Gosselin, S.I. Cho, JOM **56**, 34 (2004)
87. F. Wang, Z. Yu, K. Qi, J. Alloys Compd. **438**, 110 (2007)
88. A.A.E. Daly, A.M.E. Taher, Mater. Des. (2013). doi: http://dx.doi.org/10.1016/j.matdes.2012.12.081
89. H.R. Kotadia, O. Mokhtari, M.P. Clode, M.A. Green, S.H. Mannan, J. Alloys Compd. **511**, 176 (2012)

90. H. Fallahia, M.S. Nurulakmala, A.F. Arezodarb, J. Abdullah, Mater. Sci. Eng., A **553**, 22 (2012)
91. D.A.A. Shnawah, S.B.M. Said, M.F.M. Sabri, I.A. Badruddin, F.X. Che, Microelectron. Reliab. **52**, 2701 (2012)
92. C.L. Chuang, L.C. Tsao, H.K. Lin, L.P. Feng, Mater. Sci. Eng., A **558**, 478 (2012)
93. A.S.M.A. Haseeb, M.M. Arafat, M.R. Johan, Mater. Charact. **64**, 27 (2012)
94. B.S.S. Chandra Rao, K.M. Kumar, V. Kripesh, K.Y. Zeng, Mater. Sci. Eng., A **528**, 4166 (2011)
95. P. Liu, P. Yao, J. Liu, J. Electron. Mater. **37**, 874 (2008)
96. S.M.L. Nai, J. Weib, M. Gupta, J. Electron. Mater. **37**, 515 (2008)
97. K.M. Kumar, V. Kripesh, A.A.O. Tay, in *Proceedings of the Electronic Components and Technology Conference*, 2006, pp. 237–243
98. S.M.L. Nai, J. Weib, M. Gupta, J. Electron. Mater. **35**, 1518 (2006)
99. Y.D. Han, C.M. Tan, S.M.L. Nai, L.Y. Xu, H.Y. Jing, J Wei, in *Proceedings of the Electronic Components and Technology Conference*, 2010, pp. 979–984
100. Y.D. Han, H.Y. Jing, S.M.L. Nai, L.Y. Xu, C.M. Tan, J. Wei, Intermetallics **31**, 72 (2012)
101. Y.D. Han, H.Y. Jing, S.M.L. Nai, L.Y. Xu, C.M. Tan, J. Wei, J. Electron. Mater. **41**, 2478 (2012)
102. K. Bukat, J. Sitek, M. Koscielski, M. Jakubowska, M. Stoma, A. Mtozniak, W. Niedzwiedz, Solder Surf Mt Tech. **24**, 267 (2012)
103. K.M. Kumar, V. Kripesh, A.A.O. Tay, J. Alloys Compd. **450**, 229 (2008)
104. L.C. Tsao, J. Alloys Compd. **509**, 8441 (2011)
105. L.C. Tsao, Mater. Sci. Eng., A **529**, 41 (2011)
106. L.C. Tsao, J. Alloys Compd. **509**, 2326 (2011)
107. S.Y. Chang, L.C. Tsao, M.W. Wu, C.W. Chen, J. Mater. Sci.: Mater. Electron. **23**, 100 (2012)
108. T.H. Cheng, L.C. Tsao, F.S. Wang, W.Y. Kuo, in *Proceedings of the International Conference on Electronic Packaging Technology and High Density Packaging*, 2011, pp. 374–378
109. T. Fouzder, I. Shafiq, Y.C. Chan, A. Sharif, W.K.C. Yung, J. Alloys Compd. **509**, 1885 (2011)
110. A.K. Gain, Y.C. Chan, W.K.C. Yung, Microelectron. Reliab. **51**, 2306 (2011)